UCRL-2662

UNIVERSITY OF CALIFORNIA — BERKELEY

RADIATION LABORATORY

DISCLAIMER

UCRL-2662
Unclassified
Physics

UNCLASSIFIED

UNIVERSITY OF CALIFORNIA

Radiation Laboratory

Contract No. W-7405-eng-48

INTERACTIONS OF 28 MEV PROTONS AND HE^4

Arthur F. Wickersham

August, 1954

Berkeley, California

CONTENTS

INTERACTIONS OF 28 MEV PROTONS AND HE^4

Arthur F. Wickersham

Radiation Laboratory, Department of Physics,
University of California, Berkeley, California

August, 1954

ABSTRACT

The reactions of 28 Mev protons and He^4 have been investigated with a cloud chamber placed in the beam of the Berkeley linear accelerator. The following processes were observed:

1. p - α elastic scattering
2. $He^4(p, d)He^3$
3. $He^4(p, 2p)H^3$
4. $He^4(p, pn)He^3$

Angular distributions were obtained for the first two reactions. Comparison of the yield of the first two reactions with the results of other investigators working with the same accelerating machine permits the assignment of differential cross sections of these first two reactions and total cross sections to the other reactions.

Analysis of the rest frame momentum spectrum of protons from the (p, 2p) reaction presents no evidence of an excited level in He^4 in the energy range studied.

The reaction $He^4(p, p\gamma)He^4$ was not observed, indicating a cross section less than 2 millibarns in this energy range.

INTERACTIONS OF 28 MEV PROTONS AND HE^4

Arthur F. Wickersham

Radiation Laboratory, Department of Physics
University of California, Berkeley, California

August, 1954

INTRODUCTION

The measurement and description of energy levels has been one of the prominent activities of nuclear physicists, just as it was of atomic physicists in earlier years. It is of particular interest to know whether or not He^4 possesses any energy levels because it is the most elementary nuclear particle to exhibit saturation of nuclear forces, and in some theories of nuclear structure it is used as a fundamental building unit.

E. Feenberg [1] in 1936 predicted at least one stable excited state for He^4. This work was reviewed, and the problem further discussed, by Bethe and Backer [2] in the same year. They predicted, on the basis of what was then known about nuclear forces, three possible levels, two of which, the ^3p and the ^1p, were supposed stable at 16 Mev and 10 Mev. Bethe and Backer had available the experimental work of Crane et al. [3]: a study of the reaction of protons on Li^7 in which a 16 Mev γ-ray had been detected. One of the possible interpretations suggested by the experimenters was $p + Li^7 \rightarrow He^4 + He^{4*} \rightarrow He^4 + He^4 + \gamma$, rather than the present day interpretation $Li^7 (p, \gamma) Be^8$. Subsequent knowledge, in particular the discovery of other than ordinary forces, vitiated the early theoretical predictions.

In 1949 several experimenters [4] [5] [6] observed the reactions $n + He^3 \rightarrow He^{4*}$ using thermal neutrons. In particular King and Goldstein [4] at Los Alamos found no evidence of any excited state in He^4 in the energy region close to 20.5 Mev by observing a pure $1/v$ law absorbtion of the neutrons, where v is the velocity of the neutrons. This work was extended in 1950 by Argo et al. [7] [13], who observed the reaction $H^3 (p, \gamma) He^4$ using protons up to 2.5 Mev. They detected a group of γ-rays,

decided that $E_\gamma > 17.5$ Mev and concluded that the γ-ray yield indicated an excited state in He^4 at about 21.6 Mev with a half width of 1 Mev.

The publication of these results was quickly followed by a theoretical paper on this problem by Flowers and Mandl [8] in England. Flowers and Mandl calculated the inverse process - the photodisintegration of He^4 - and used a phase space inversion to compare their theory with the Los Alamos data. Their results indicated that it was possible to explain the Los Alamos γ-rays as the yield from the beginning of an electric dipole emission spectrum, thus the introduction of a He^4 excited state was possible but not demanded.

In 1952 a comprehensive search for an excited state was completed by J. Benvenisti [9] at Berkeley. Using a counter telescope Benvenisti detected protons and deuterons scattered from a 31.5 Mev linear accelerator proton beam by a helium target. He found no evidence of excited states in the energy region he was able to investigate. Because of the energy cut off limit required by the counter telescope Benvenisti would not have been able to detect a small group of protons having a range less than 50 mg/cm^2 (5 Mev). Thus, for example, if there were an excited state at 23 Mev, the recoil protons would not have been visible because their energy would have been to small.

Since the cut off point of Benvenisti was rather close to the region in which the Los Alamos workers suspected an excited state, it was deemed desirable to confirm and extend his results. By using a cloud chamber it is possible to detect inelastic protons having a range greater than 1.8cm. (0.6 Mev). This would permit observation of an excited state below 23 Mev.

The cloud chamber technique is capable of associating the inelastic protons with the various types of reactions that produced them, thus minimizing background and possibly giving more information about the nature of the inelastic events.

II. EXPERIMENTAL PROCEDURE

Figure 1 shows a plan view of the experimental geometry. The Helmholz coils J were set up in an annex to the main building. A steering magnet C directed the beam down twenty feet of evacuated brass tubing and through a port in the wall of the building and into the chamber.

In the annex it was found necessary to use iron pipe to shield the beam from the return field of the Helmholz coils. The iron pipe was fastened rigidly to cement blocks because it was subject to large forces whenever the Helmholz coils were pulsed. Initially the position of the pipe and the method of collimation were changed several times in the effort to obtain the best possible spray free beam. The arrangement finally used is shown in Fig. 1 and consists of a 100 mil diameter carbon collimator D at the after edge of the steering magnet. Fifteen feet beyond the steering magnet at the junction E of the brass and iron pipes there was placed a second collimator 1/8 inch in diameter. This collimator was shadowed by a third collimator, 5/32 inches in diameter, placed one foot beyond the second.

Since the linear accelerator is capable to producing a hundred to a thousand times as much beam as the cloud-chamber can tolerate a fourth collimator B , with adjustable jaws and placed before the steering magnet, was used to decrease the beam intensity to operating level. At the same time it was necessary to provide an ionization chamber, open to the atmosphere for minimal stopping power, so that the accelerator operator could continually adjust the accelerator for the proper maximum intensity to maintain a constant beam pulse size in the cloud chamber.

The Helmholz coils J produced a 7,000 gauss field when used in pulsed operation. They were pulsed by a 550 kw minesweeper generator with a two ton flywheel mounted on the shaft between the generator and the motor. The field pulse, which was synchronized with the cycle of the cloud chamber, had a rise time of 2-1/2 seconds and remained stationary at its peak for about 0.2 seconds.

The cloud chamber I consisted of cylindrical front and back

volumes of 16 in. outside diameter. The front volume was 6 in. deep and separated from the back volume by a black velvet covered lucite disc mounted on pantograph arms. The back volume emptied to atmospheric pressure through a pop valve. The front volume was filled with 1 1/3 atmospheres of Helium and water vapor; the back volume was supplied with compressed air through pressure regulator valves to provide an expansion ratio of approximately 20 percent.

The photographs were taken with a specially constructed stereoscopic camera M taking 100 foot strips of 1.8 in. Eastman Linographic Ortho film per loading. It was mounted on a light tight tube L with its focal point 52 in. from the center of the front volume of the chamber. The pictures were taken at f-11 with the chamber illuminated by two General Electric FT 422 flash tubes each of which was fired by a 512 mfd. capacitor bank charged to 1500 volts. Two examples of the photgraphy are given in Figs. 2 and 3.

After development the film was reprojected on an apparatus which optically reproduced the geometry of the original photography, the life-size images appearing on a translucent screen. This reprojector used the lenses originally used in the camera. The light sources for reprojection were blower-cooled type 300K Western Union arc lamps. The reprojector is sketched in Fig. 4 and a more detailed description is given in reference 10.

In this experiment the beam from the linear accelerator ran for 400 microseconds at intervals of 1.33 seconds. The beam was interrupted 2-1/2 seconds before the expansion of the cloud chamber and pulsed once upon completion of the expansion. Several seconds later the beam was turned on again so that it could be monitored by the operators until the next operation of the cloud chamber.

Interruption of the beam was accomplished electronically by shifting the ion source pulse out of phase with the rest of the accelerator, thus everything remained operative but no beam was produced. When the cloud chamber had completed a fast expansion the ion source was shifted back into phase for one pulse, sending protons through the expanded chamber. The proton pulse was preceded in time (0.133 seconds) by a signal from the accelerator which was in phase with the duty cycle of the accelerator and therefore could be used to start the

timers that controlled the cloud chamber cycle.

Full expansion was attained 2 milliseconds before the proton beam traversed the cloud chamber and the lights were flashed 35 milliseconds after arrival of the protons.

In the 1-1/2 minute intervals between fast expansions the linear accelerator was run continuously at full beam so that the operator could adjust the accelerator to maximum beam with the aid of the ionization chamber shown in Fig. 1. In this interval the cloud chamber was given two slow expansions.

It was found that it was possible to take pictures at the rate of one every 1-1/2 minutes, this limit being imposed by the maximum rate at which heat could be removed from the Helmholz coils.

III. ANALYSIS

The most abundant reaction that takes place when protons are scattered in helium is the elastic p - α scattering. Fortunately this is also the reaction easiest to recognize. Figure 5 is an enlargement of an actual beam photograph. The elastic process is manifested in a long, thin, lightly ionizing track associated with a relatively short, thick, heavily ionizing one. The uniqueness of appearance is due in part to the extraordinarily high reaction energies associated with He^4. It takes about 19 Mev. to remove the first nucleon from helium, and since only 27.9 Mev is available, no inelastic process can have a lightly ionizing particle associated with it. The relative ionization of the beam protons is 10 times minimum ionization and that of the elastically scattered protons is 10 to 30 times minimum, while particles from inelastic reactions, because of their low kinetic energies, have relative ionizations of 100 to 600 times minimum, or greater. Thus the elastic scatter is uniquely characterized by a track almost as lightly ionizing as the beam tracks and associated with a second heavy track that is always 400 or more times minimum.

Furthermore the angular separation of the two prongs of an elastic scatter is always greater that 90°, while the angular separation of prongs associated with inelastic events is rarely greater than 90° because of the large velocity of the center of mass system. These two characteristics, ionization and angular separation, together with the requirement of coplanarity of the two prongs (a requirement on all two body processes) permitted immediate visual identification of elastic processes, and thus more than two thousand elastic scatters were rapidly separated from the residual data. Subsequent analysis of the residual data disclosed that only two elastic scatters had been overlooked in this initial indentification.

In order to obtain the angular distribution of the protons in the center of mass system it is necessary to measure θ_p, the scatter angle of a proton in the laboratory system, and then to transform this angle into θ'_p, the angle in the center of mass system. The assumption was made that the protons entered with 27.9 Mev energy.

The laboratory scatter angle was determined in three different ways: by direct measurement, by measuring the angle $\Delta = \theta_p + \theta_\alpha$ between the alpha particle and the proton, and by measuring the range of alpha particles that stopped in the gas of the chamber. The third method alone was used when helium recoils stopped in the gas, and the second method when this did not occur. Cross checks of these methods were made frequently and are discussed in Section IV.

There are three reasons why the analysis of the elastic scattering data is important: the elastic scattering absolute cross section measurements made in counter experiments[11] permits the assignment of absolute cross sections to other reactions studied here; comparison of angular distribution with that obtained by counters checks the cloud chamber technique for systematic errors; the complete measurement and analysis of a two body event provides several internal checks and corrections. The analysis of elastic scatters allows one to correct for loss of events with increasing azimuthal angle (loss due to decreasing visibility) and loss of events at small distances from the walls of the chamber. Further, this analysis provides an indication of the errors involved in the measurement of scatter angles, and insight into the geometry of the experiment was obtained by observing the loss in numbers of events due to their obscuration by the proton beam.

In summary, the primary reason for analyzing the elastic scatters was to check the geometric factors which obscure particles and affect accuracy of measurement of angles. An angular distribution of the elastic scatters was obtained as a by-product of this effort and is of some interest in itself. The results are given in Section V.

A less frequent type of event, but one even more readily identiable, is the elastic proton-proton scatter arising from the water vapor present in the Chamber. This type of event was identifiable at sight by it obvious characteristics: 90° angular separation of the two prongs, coplanarity, and low relative ionization (10 to 30 times minimum) of both prongs. Only a few of these were measured as a check on the accuracy of θ and α measurements. Their number was counted and found to be consistent with the amount of water vapor in the chamber as determined from temperature-water vapor pressure

tables.

The presence of water vapor also resulted in several elastic proton-oxygen scatters. Their characteristics were identical with those of the elastic p - α scatters with the exception that the recoil nucleus was much more heavily ionizing and had a much shorter range. Because of the shortness of the recoil range and the thickness of the beam, only a small fraction of these were seen as two prong events. No attempt was made in this experiment to count and identify single prong events.

In summary it can be said that all of the elastic processes were easily and rapidly separable. The residual data - some 282 inelastic reactions - required more extensive analysis for identification.

The most prevalent inelastic reaction observed was the inverse Butler,[12] or pickup deuteron process, $He^4(p, d)He^3$. Fortunately this was also the easiest of the inelastic reactions to identify. By examining a list of the inelastic reactions possible at this energy -

$$He^4(p, d)He^3$$

$$He^4(p, pn)He^3$$

$$He^4(p, p\gamma)He^4$$

$$He^4(p, 2p)H^3$$

- one sees that with the exception of the third only the first is two body, or coplanar. The third reaction is not strictly a two body process, but because of the relatively small amount of momentum associated with the gamma ray it frequently might appear to be two body. Thus all inelastic scatters with two (visible) prongs coplanar within 180 ± 5 or 6 degrees of azimuth were separable as possible pickup deuteron events.

In the above list only the first three reactions produce a doubly charged fragment. Now if one expresses momentum in units of the $B\rho$ measured for singly charged particles, $p = B\rho$, where B is the magnetic flux in gauss and ρ the radius of curvature of the particle in centimeters, then one must put $p = 2B\rho$ for doubly charged particles. Thus if one can balance transversely the momenta associated with the prongs of a two pronged event by doubling the measured $B\rho$ of one of the prongs: $B\rho_1 \sin\theta_1 = 2B\rho_2 \sin\theta_2$, when the prongs are coplanar, then that

event is identified as the $He^4(p, D)He^3$ reaction. As a further check, if $B\rho_1 \cos\theta_1 + 2B\rho_2 \cos\theta_2 = B\rho_o$, where $B\rho_o$ is the momentum of a beam proton, then the reaction can be identified as a pickup deuteron process, possible but unlikely exceptions being those cases in which two prongs of a three body event accidentally appear to be coplanar within the errors of measurement.

We have one more clue that will establish the identity of this reaction, namely the known energy of the beam. The sum of the kinetic energies of the fragments and the Q of the reaction must equal 27.9 Mev.

The three conditions discussed so far - coplanarity, momentum balance and energy balance - were all that were needed to identify the 185 pick-up deuteron events observed. However there was further information available that often simplified the identification procedure. Whenever a fragment stopped in the gas of the chamber so that its range could be measured along with its curvature, then it was possible to identify the particle from $B\rho$ - range curves. Often, when a fragment did not stop in the chamber, the knowledge that its range was equal to or greater than the portion seen in the chamber was sufficient, together with its curvature, to eliminate one or more possibilities. In addition, an estimate of the relative ionization of each fragment frequently helped to identify or corroborate identification of particles and events.

In the center of mass system the recoils from a two body collision have equal and opposite momenta. In this experiment the initial beam energy is constant and therefore in the c.m. system all of the deuteron and He^3 recoils from pickup reactions will have the same momentum. The momenta of the recoils associated with events identified as pickup processes were transformed into the center of mass system and the results of this transformation are shown in Fig. 6. The results were not only useful as a check on the identification procedure but also provided a relatively accurate determination of the beam energy. The relatively high accuracy is due to the fact that small energies of a few Mev were determined experimentally and the beam energy was computed from these small energies by adding to them the large (19 Mev) mass difference of the reaction, the mass difference being known quite ac-

curately from mass spectrograph measurements. The experimental errors causing the spread in momentum shown in Fig. 6 are discussed in Section IV.

After identification of pickup processes the remaining 97 events could consist of only the following three reactions in He^4: (p, 2p), (p, pn), and (p, pγ). There was not enough energy in the beam to produce reactions more intricate than those listed.

The first two reactions were difficult to distinguish from one another chiefly because one of the prongs in the (p, 2p) reaction frequently was obscured by the proton beam. The identification technique employed was much like that discussed above, involving transverse and longitudinal momentum conservation, energy conservation, estimation of relative ionization and frequently the identification of fragments from curvature and range measurements. There was this difference: when only two of the three prongs were observed, the energy and momentum balance must direct the unseen particle into a region of space in which it could not have been seen. Of course this criterion does not apply in the case in which the third fragment is the non-ionizing neutron, but even so it was sometimes useful in separating the triton and He^3 reaction by elimination of the triton possibility.

This procedure resolved the remaining data into 58 He^4(p, 2p) H^3, 9 He^4(p, pn)He^3 and no He^4(p, pγ)He^4 reactions, and a final residuum of thirty events analyzed as follows:

21 events which were probably protons colliding inelastically with oxygen

7 elastic proton-helium scatters of degraded energy

2 non-identifiable reactions

The inelastic oxygen reactions were recognized by their having properties not attributable to helium reactions. For example, a four or five prong event or one having three very heavily ionizing prongs could not be caused at this energy by an interaction with helium, but rather with some heavier nucleus. Of course these events were not positively identified as oxygen events but simply as interactions with nuclei heavier than helium or hydrogen. There is no reason to suspect the presence of any contaminant other than the oxygen in the water vapor.

Those events that were at sight obviously not helium events were

not analyzed, but those that were not so recognizable were recorded for analysis along with the rest of the inelastic data. This latter group constitutes part of the 21 events listed in the above table, where some of the 21 may be mere accidental conjunctions. Of these 21 events 9 were so classified because the observed scatter angles were much too large to allow momentum balance in the forward direction without requiring more energy than that available to helium reactions, 1 event because it had two prongs both identifiable as having a mass of 3 or 4 relative to the proton mass, 1 event because more than 3 prongs were required to balance momentum and ten events were so classified as a result of more complicated analysis.

In two cases the analyzed data did not permit a reasonable best choice from among the possible helium reactions, and these are listed above as non-identifiable.

The work of Argo and others at Los Alamos [7] [13] indicated that the reaction $H^3(p, \gamma)He^4$ existed and suggested the possibility of a level in helium in the region of 21 to 23 Mev. Since 28 Mev protons can supply enough energy to the center of mass system to produce an excited state of He^4 in this energy range a search was made for the reaction $He^4(p, p\gamma)He^4$, but no events were found that could be identified as such. Since the reaction $He^4(p, d)He^3$ can imitate the approximate coplanarity of the gamma ray reaction and can also imitate it in relative ionization, and additional study of all (p, d) events was made.

The momenta of all the deuterons were transformed to the center of mass system where their values were found to group around 3.1×10^5 gauss centimeters. Now if there were a level in the 21 to 23 Mev region, and if this level decayed by gamma emission, and if the momenta of the excitation protons associated with such a process were mistakenly transformed into the c.m. system as deuterons from a (p, d) reaction, then their transformed momenta would have appeared in the region of 0 to 2.1×10^5 gauss centimeters. No such momenta appeared.

A similar statement cannot be made concerning possible confusion of $(p, p\gamma)$ events with (p, 2p) events. However it will be seen from the c.m. momentum spectrum of (p, 2p) protons, to be discussed in Section V, that no significant contribution to that spectrum could have been made by protons of constant momentum.

In addition at the close of the analysis all of the remaining in-

elastic reactions - (p, 2p) and (p, np) - were specifically reexamined for any possible (p, pγ) reactions but none was found. A reexamination of the residuum disclosed nothing that reasonable could be identified as a (p, pγ) reaction. Most of the inelastic oxygen events were obviously not reactions of any type in helium, and the elastic proton-helium events of degraded energy all had kinetic energies between 20 and 25 Mev - energies much higher than the 5 or 6 Mev kinetic energy allowed to a proton and alpha particle after a 21 to 23 Mev gamma ray has left the system.

IV. ERRORS AND CORRECTIONS

A. Range

It has been shown that the identification of an event necessitates measurements of radius of curvature, range, magnetic field strength, position of origin and scatter angle θ.

The range of a particle stopping in the gas was determined to within 3-1/2 millimeters. Of this error 3 millimeters was due to the uncertainty of the position in the beam of the origin (a point that must be determined for each event by reprojecting two or more prongs back to their intersection) and an average of two millimeters due to straggling. In order to determine energy or momentum from range one must know the stopping power of the gas as well as the nature of the particle. For this calculation it was necessary to know the temperature and pressure of the gas. The pressure was determined to ± 1/2 centimeter of Hg by an open tube manometer and subsequently corrected to atmospheric pressure by barometric readings taken concurrently. Temperature was read on a mercury thermometer taped to the outside of the glass wall of the front volume of the chamber. It was readable to within 1^{o}C, but the actual temperature inside of the chamber before expansion may have differed as much as $1^{o}$from the value read.

An internal check on the range-energy calculation was provided by measuring the range and angle of recoil elastic alphas that stopped in the gas. Since the beam energy E_o is known the scatter angle θ of the alpha particle is given by

$$\theta = \cos^{-1}\left(\frac{5}{4}\sqrt{\frac{E_a}{E_o}}\right)$$

where E_a is the energy of the alpha particle. (See Appendix A). Comparison of the scatter angle obtained from the range with the scatter angle measured directly showed a mean difference of ± 1.8^{o}.

This observed mean difference can be accounted for in the following way. Because of the rapid variation of range with energy in helium, the energies and momenta of the particles can be determined rather accurately from range measurements. Thus the 3-1/2 mm. error in

range measurement produces at most only .03 to .09 Mev error in the energy of protons and alpha particles, respectively, that stop in the gas. If we take the logarithmic derivative of the above equation with respect to θ and put dE = .09 Mev, E_α = 2 Mev, we find that $d\theta \approx \pm 0.5^\circ$ This may be regarded as a typical error in θ due to error in range.

The expected error in the direct angular measurement of the recoils, determined by the methods discussed in the remainder of this section, is 1.5°. This is smaller than the error usually expected because these tracks were especially selected for this range energy check. When this error is combined with the $\pm 0.5^\circ$ error obtained above we get $\pm 1.6^\circ$, which is in good agreement with the observed mean difference between the two methods of $\pm 1.8^\circ$.

This agreement implies that the error in the results of the range energy calculations produces negligible error in the scatter angles determined from the range of stopping alpha particles. Other than this determination of scatter angle of elastic scatters from recoil alphas that stopped in the gas, the range energy relation was used only to provide a correction term in the measurement of $B\rho$ and for occasional particle identification by comparison of $B\rho$ and range. All of these applications are quite insensitive to error in the range energy relationship therefore its accuracy will not be discussed beyond stating that the stopping power determined from elastic alphas indicates that the error in the value calculated from pressure and temperature is not greater than ±5 percent.

The internal check just described also indicates that there was no gross contamination of the target since helium has the least stopping power of any gas. This evidence is further substantiated by the observed yield of proton-proton elastic collisions and collisions involving nuclei heavier than helium. These yields were consistent with that to be expected from the water vapor present assuming a reasonable proton-oxygen cross section.

B. Magnetic Field

The magnetic field strength was determined by recording the peak current reading of each pulse during the running time of the experiment. After the experiment the field was measured with a search

coil and integrator. These were electronically synchronized with the cloud chamber cycle so that they measured the field value at the instant the beam pulse of protons traversed the chamber. Measurements were taken throughout the volume occupied by the cloud chamber. The search coil and associated equipment was calibrated in a test field which was measured with a proton magnetic moment apparatus. The results thus obtained expressed magnetic flux density in terms of current readings taken on the same ammeter used in the course of the experiment. A graph of the uniformity measurements, showing flux density per unit current across the horizontal diameter in the mid-plane between the Helmholz coils, is shown in Fig. 7. The overall inaccuracy of the field measurement was ± 1/3 percent, which is small compared to the errors in the curvature measurements of individual tracks.

C. Radius of Curvature and Angular Measurements.

The dip angle α, beam angle β and radius of curvature of a track are measured in the following manner. The horizontal axis of rotation of the translucent screen is placed perpendicular to the starting point of the track. If this is not visible because it is obscured by the proton beam then it is placed perpendicular to some convenient point on the track. The screen is raised or lowered until the two images from the two stereoscopic pictures coalesce on the axis of rotation. Then the screen is tilted through the angle α from the horizontal until both images coalesce along the full length of the track. The screen then follows the track except for a slight error due to the helical path of the track in the magnetic field. Arcs of different radii drawn on transparent lucite templates are matched to the curved track images over a length selected to permit most accurate comparison. From the result of several tests it has been our experience that the error made in this measurement never exceeds 0.1 millimeters in the sagitta, irrespective of the particular curvature and track length available.

The lucite templates are drawn with normals to the arcs when they are manufactured. After the radius of curvature has been determined the normal to the appropiate arc is placed on the horizontal axis of rotation of the transparent screen, and the screen is moved until its horizontal axis and the intersecting arc are at the origin of the event.

The translucent screen is then rotated about its vertical axis until the arc on the template coincides with the track being measured. Thus by reading the angle on a scale attached to the vertical axis of rotation one measures the complement of the beam angle β.

We have just defined the dip angle α and beam angle β in terms of the operation of measurement. These angles, along with the other coordinates used in cloud chamber measurements, are also defined in Appendix B and in Fig. 8. For convenience we repeat them here. The dip angle α is the angle a track makes with its horizontal projection, and the beam angle β is the angle between the horizontal projection of a track and the beam. Thus β is the horizontal projection of the scatter angle θ, where θ is the angle between the track and the beam. The plane containing a track and the beam is called the azimuthal angle ϕ is the angle of the azimuthal plane of the track, or in the case of a two body collision the azimuthal plane of the event. The azimuthal angle ϕ is the angle of the azimuthal plane to the horizontal plane. These angles are also defined in Fig. 4, an isometric drawing of the reprojection equipment.

The accuracy of reprojection and measurement with the equipment used has been thoroughly investigated by W. Powell and collaborators[10]. They concluded that beam angles could be determined to $\pm 1^{\circ}$ if the origin of the track is visible. The errors in this experiment are larger than those given by Powell because the beam obscures the origins of the tracks. Experience has shown that the errors in dip angle α are consistent with the assumption that the height of the track ends can be determined to within $\pm$1mm. for $0 < \alpha < 50^{\circ}$. The overall error in determing θ can be estimated by considering the results of measurements on ten elastic p-p scatters, for which the angular separation of the prongs, Δ, should very closely equal 90° at this energy:

$\Delta = \theta_1 + \theta_2$	Deviation	
91.1	1.1	
92.5	2.5	
89.8	0.2	
90.2	0.2	
91.5	1.5	
90.0	0.0	
90.2	0.2	
89.8	0.2	
88.2	1.8	
88.3	1.7	
90.2°	0.9°	average values

Column 1 indicates Δ as determined from

$$\cos \Delta = \cos \Delta' \cos \alpha_1 \cos \alpha_2 - \sin \alpha_1 \sin \alpha_2 \qquad (1)$$

where $\Delta' = \beta_1 + \beta_2$ is the horizontal projection of Δ and is independent of initial beam direction. Δ', α_1 and α_2 are the measured quantities. Column 2 lists the differences between Δ and 90°.

Notice that here, as in the case of elastic proton-helium scattering, Δ is not measured directly but found from measurement of angle $\Delta' = \beta_1 + \beta_2$ and dip angle α by means of equation (1) above. In the case of a single prong equation (1) reduces to

$$\cos \theta = \cos \beta \cos \alpha \qquad (1')$$

The factors that make it difficult or impossible to measure Δ or θ by tilting the space table into the azimuthal plane are discussed in Appendix C.

The errors in the proton-proton elastic scatters above are smaller than in most other events for the following reasons. The protons are of such energy that they never stop in the gas, hence both prongs are always long (15 to 30 centimeters) and errors due to scattering are minimal; their relative ionization is low (10 to 20 times minimum) and thus they can be sharply focussed; and finally they are coplanar, which allows easier and more accurate determination of their intersection or origin. The θ's of noncoplanar inelastic events may have errors two or three times the size of those of the proton-proton scatters. Measurements on short stubs (1-1/2 to 3 centimeters) are estimated to produce errors in θ as high as $\pm 5^\circ$ to 10°.

Another source of error in θ is the divergence of the beam as it traverses the chamber. Since the actual core of the beam enlarges from 1/4 to 3/4 inches over its 35 centimeter long path in the cloud chamber, it is readily deduced that the beam protons can diverge at most 1.0° from the median line and that the average error is less than $\pm 1/2^\circ$.

Before we can conclude the discussion of error in θ it is necessary to consider errors in both θ and radius of curvature caused by turbulence and scattering. The Cartesian coordinates of straight tracks obtained from no-field pictures were measured with a travelling microscope. Tracks were measured that were from the same picture,

parallel and separated by less than 1/4 inch and that traversed almost the entire length of the chamber. Large deviations from straight lines were found that were due to scattering. It was concluded that the smaller fluctuations from straight lines indicated the limit of resolution of measurement since no correlations in deviation were noticed between the parallel tracks. Thus it was concluded that turbulence errors were less than the resolution of the measurements, i.e. gave spurious radii of curvature of more than approximately 200 meters, and that error due to turbulence was negligible compared to error from scattering.

Comparison of measured values of $B\rho$ with the value expected for the two body reaction $He^4(p,d)He^3$ (see Fig. 6 for example) indicates a mean error in the average per event of the momenta of deuterons and He^3's of about ±4 percent. For other inelastic events a comparison of the total kinetic energy of the fragments, as determined by $B\rho$ measurements, with the expected energy also indicates an average error in $B\rho$ of about ±4 percent. The mean deflection of a 2.5 Mev proton due to multiple scattering calculated from Bethe's[4] formula gives ±3 percent error in radius of curvature. Thus most of the observed error can be accounted for by scattering. If in addition we take our previous result for error in measurement of ρ, 0.1 millimeters error in the sagitta, then for a typical track (ρ = 30 centimeters; length chosen for measurement: 10 centimeters) the error in measurement will be 2.4 percent. Thus the total error in ρ for a typical track will be ±3.8 percent, in good agreement with the observed average value of ±4 percent.

The error in ρ due to scattering will cause error in the measurement of beam angle since the track must be projected back through the opaque beam to the origin of the event. Let β_e be the beam angle that the track makes at the visible edge of the beam, then

$$\beta = \beta_e + \frac{L}{\rho}$$

where β is the beam angle at the origin of the event, L the distance along the track from the edge of the beam to the origin of the event and ρ the radius of curvature of the track. If primes denote measured quantities then one can obtain from the above equation:

$$\beta - \beta' = L \frac{\rho' - \rho}{\rho\rho'} \text{ or}$$

$$\Delta\beta = \frac{L\Delta\rho}{\rho^2} .$$

For a typical inelastic track L = 3 centimeters, ρ = 30 centimeters and $\Delta\rho$ is 4 percent of 30, or 1.2 centimeters. This gives a typical error in β of 0.2 degress.

Of course if deflections occur before the particles emerge from the beam then even though these deflections would not contribute to error in ρ they would result in error in θ, and if large enough would make identification of the event by momentum and energy conservation difficult or impossible. But the probability of a 2.5 Mev proton, a typical inelastic track, suffering a single Rutherford scatter of 2.5° or more if it travels 2 cm. before emerging from the beam is less than 1 in 1200. The root mean square deflection due to multiple scattering of a 2.5 Mev proton before it emerges from the beam is only 0.21°.

The total error in θ, consisting of 2.5° due to errors in measuring α and β, 0.5° due to beam divergence 0.2° due to error in measuring ρ, 0.2° due to scattering and 0.5° in determining the initial direction of the beam, is taken to be about $\pm 2.7^\circ$. This is for a typical track. It is obvious that some tracks-the proton-proton and proton-helium elastic scatters for example - can be measured much more accurately, but 2.7° error is expected to be average for the low energy tracks characteristic of inelastic reactions.

We have described the operation of measuring ρ and discussed error in ρ due to scattering and turbulence. There is in addition a systematic error that must be corrected by use of the range-energy relation. Since a particle loses energy from the origin of the event to the point of measurement it is obvious that the radius of curvature measured will be too small. $B\rho$ - range curves were constructed on the basis of the range-energy relation, then from the measured value of $B\rho$ and the known distance from the origin of the event to the center of the region of measurement the initial momentum of the particle was determined.

The magnitude of these corrections was usually 2 to 3 percent, occasionally as high as 6 to 8 percent. Corrections of greater magnitude usually could occur only for particles that stopped in the gas, and the momentum of stopping particles was more readily and accurately determined by range alone. Because of the smallness of these corrections any error in them due to error in determination of the range-energy relation is negligible.

D. Beam Direction

Knowledge of the initial beam direction was not essential for the analysis of the elastic events since the analysis could be carried out in terms of $\Delta = \theta_1 + \theta_2$, a quantity insensitive to beam direction.

For the analysis of three body events it was necessary to know the beam direction at the origin of each event. This was accomplished by measuring a running coordinate S, the distance along the beam between the origin of the event and the point at which the beam enters the cloud chamber. Then if one knows β_o the initial direction of the beam as it enters the chamber and the angular deviation of the beam per unit length of beam, the beam direction at the origin of the event is immediately known from the relation

$$\beta = \beta_o - S \frac{\Delta\beta}{\Delta S} \quad . \quad \text{(Fig. 20)}$$

β_o and the constant $\frac{\Delta\beta}{\Delta S}$ were accurately measured on an exceptionally weak beam pulse containing only a few protons. A template with the appropriate curvature was matched to the beam and the horizontal axis of the space table aligned with the normal to the curve at the point where the beam entered the chamber. The horizontal scale of the space table was then permanently locked in the position $\beta_o = 0$. The error in this determination was $\pm 1/2^o$. The value of $\frac{\Delta\beta}{\Delta S}$ was determined from the curvature to be 0.50 degrees per cm, thus making this an easy correction to apply.

It has already been mentioned that the uncertainty in the position of the origin of an event was about 3 millimeters. This is also the uncentainty in measuring S, the distance along the beam from the edge of the chamber to the origin of the event (see Fig. 9). Because $\frac{\Delta\beta}{\Delta S}$ for the beam itself is small the resultant error in the correction to θ,

due to error in S_1 is only $\pm 0.15^{o}$.

E. Beam Energy

Several methods were available for determination of the beam energy. Of these the determination of the momenta of the two $He^4(p, d)He^3$ fragments by measurement of their $B\rho$'s leads to the most accurate value. This method takes advantage of the large mass difference (18.3 Mev) for the reaction, a quantity very accurately known from mass spectrometer measurements. Thus in effect only a fraction (1/3) of the determination is subject to the errors of this experiment.

If the beam is mono-energetic then because of the two body nature of the deuteron pickup process the center of mass momenta of the fragments will be equal and unique. Thus it would be convenient to determine the beam energy from the center of mass momentum spectrum of this reaction. A good determination was obtained by plotting the average momentum per event, i.e. the average of the He^3 and deuteron center of mass momenta. The spectrum so obtained is shown in Fig. 6. The mean value of the beam energy obtained from this spectrum is 27.88 Mev where half of the determinations fell within ± 0.36 Mev (± 0.12 gauss cm) of the mean. The energy of the initial protons was assumed to be 30.5 Mev. Then after transformation to the corresponding center of mass system the average momenta of He^3 and deuteron gave an energy for the beam of 28.2 Mev. This process was repeated using the lower value for the energy of the beam until the energy derived from the momenta agreed with the energy assumed for the transformation.

The spread of values in the pickup deuteron center of mass momentum spectrum can be completely accounted for by the spread expected from errors in measurement. Therefore it is reasonable to assume that relative to this experiment the beam was mono-energetic.

The bean energy was also determined from the curvature of the beam as it traversed the chamber, the curvature being determined from several measurements of the beam sagitta made with a travelling microscope. The result was multiplied by the average of the flux density over the center eight inches of the chamber to obtain the beam

momentum. The momentum so obtained corresponded to a proton energy of 28.2 ±0.5 Mev.

One of the better alternate methods for determining beam energy results from comparing the laboratory scatter angles of the two fragments from the pickup reaction. The result obtained by averaging over all of the pickup events observed is 28.4 Mev, where half of the 169 determinations fell within ±0.7 Mev of the mean. A weighted mean of this and the above result was not used. Instead the value obtained from the momentum spectrum was used because the major results of this experiment are momenta spectra and are sensitive to choice of beam energy. The other results of this experiment-angular distributions and total cross sections - are relatively insensitive to choice of beam energy.

F. Angular Distribution and Visibility Corrections.

Geometrical calculations show that in the proton-helium elastic process, where the protons are scattered between 25° and 170° in the center of mass system, all events are visible over an azimuthal angular range of $\pm 45^{\circ}$. This was verified in the forward direction by comparing the angular distribution with that obtained by Cork[11] as shown in Fig. 10, where the dashed lines indicate the limits of visibility.

Figure 11 is a plot of 500 elastic proton-helium events against azimuthal angle. This shows no significant decrease below 45°. Figure 12 is a plot of those 130 of the 500 proton-helium events with azimuthal angles from 45° to 75°. This angular distribution in θ would be expected to fall off at the extremes of θ. The fact that there is no fall off greater than that shown in Fig. 10 indicates that events between $\pm 45^{\circ}$ in azimuth and between 25° and 170° in θ are always observed.

All inelastic events that could be seen were measured regardless of ϕ. The 45° restriction was applied to inelastic events when their yield was being compared to other types of reactions and in computing absolute cross sections.

The first 500 elastic events were also used to determine restrictions on S, the position of origin of each event. A plot of number of events vs. S remained reasonably constant for 5 cm. $\leq$ S $\leq$ 25 cm.

The final limits applied to all events were $0 \leq S \leq 25$ cm. Plots are given in Figs. 13 and 14 for those events of the 500 for which $-45^{o} \leq \phi \leq 45^{o}$ and $0 \leq S \leq 25$ cm. concurrently.

Because of the curvature of the beam the geometry of the experiment is not symmetrical. The volume of the chamber was divided into four quadrants: upper and lower on convex and concave sides of the beam. These four quadrants can be represented as the four quadrants of a plane on which ϕ is plotted against S. The first 500 elastic events were then plotted as points on this plane. Within the limits chosen, $S \leq 25$ cm. and $\phi \leq \pm 45^{o}$, the density of points did not statistically deviate from uniformity, or randomness. This indicates that uniform sensitivity over the chamber volume was not influenced by the lack of geometric symmetry.

From the azimuthal limitation $\phi - \pm 45^{o}$, the known number of visible, i.e. ionizing, prongs for each type of event and the knowledge of the polar visibility one can calculate the probabilities that the various events will be seen as two or three prong events. These probabilities are to be used as normalizing factors in comparing yields of the various reactions and in computing total cross sections. Because these probabilities are intimately related to the type of inelastic rest frame momenta spectra that might be observed it is more convenient to discuss their computation along with the experimental results given in the next section.

V. RESULTS

A. Elastic Proton-Helium Scattering.

The center of mass proton distribution resulting from elastic proton-helium scatters is given by the circles in Fig. 10 for $\theta' = 25^\circ$ to $\theta' = 170^\circ$. Vertical lines on all cloud chamber results indicate probably errors. Crosses represent the results obtained by Cork[11] using a counter telescope. A minimum occurs at $\theta' \approx 115^\circ$ followed by a gentle rise due to exchange type interactions. No attempt was made to subtract Coulomb scattering from the forward peak. The normalization at 27.9 Mev was achieved by interpolation between Cork's results at 31.6 Mev and 19.5 Mev.

The normalization was carried out by means of a least mean square adjustment of cloud chamber and counter data in the region of $\theta' = 25$ to 55 degrees. This region was chosen because it is reasonably removed from the forward direction where events may be missed, it is a populous part of the spectrum and it is a region in which the results can be approximated reasonably by a straight line. The result obtained and used in the construction of Fig. 10 is $\frac{d\sigma}{d\Omega} = 0.1643N$, where $\frac{d\sigma}{d\Omega}$ is in millibarns per steradian and N is the number of events seen in the cloud chamber in a ten degree interval of θ and in an azimuthal range of $-45^\circ \leq \phi \leq +45^\circ$.

From this result one can compute the normalization factor for total cross section. It is $\sigma = 0.1802 \left(\frac{\Phi}{H}\right) n$, where σ is in millibarns, n is the cloud chamber event count and the factor $\left(\frac{\Phi}{H}\right)$ corrects for the limited visibility in azimuth ϕ and polar angle θ.

B. $He^4(p, d)He^3$ Collisions.

The center of mass angular distribution from 36° to 131° for pickup deuterons, $He^4(p, d)He^3$, is given by the circles of Fig. 15. Crosses are the results of Benvenisti[9] using a counter telescope, and the solid line is given by Butler's theory[12]. Since the spin of He^4 is known the results are of little interest other than to check the the reliability of the cloud chamber and to note the expected deviation from theory at large scatter angles. For the cloud chamber points the vertical scale indicates differential cross section from normalization to the elastic scattering results. The agreement is seen to be satisfactory insofar as relative position of maxima and minima are con-

cerned. Comparison of cloud chamber and counter telescope results indicates a cross section decreasing with energy.

C. $He^4(p, 2p)He^3$ Collisions.

The laboratory angular distribution for inelastic protons from the reaction $He^4(p, 2p)H^3$ is shown in Fig. 16. It shows no structure other than a general preference for the forward direction, a result expected in consideration of the rather large forward velocity of the rest frame. A differential cross section in θ cannot be given for this event because of the several ways in which it can be observed: as two protons; one proton and one triton; two protons and one triton. A total cross section is given in Table I, page 35 . In only 10 out of the 58 of these events observed were all three particles visible.

The center of mass proton momentum distribution of the (p, 2p) events, Fig. 17, shows a peak at $B\rho = 1.8 \times 10^5$ gauss centimeters or about 1.6 Mev. The authenticity of this peak and its possible causes are discussed in the following paragraphs.

There is the possibility that the peak results from a class of two body events wrongly identified. The proton momenta from elastic p-α collisions are too great to fall in this range. It must be pointed out however that in the center of mass system the reaction $He^4(p, d)He^3$ produces He^3 recoils with a $B\rho$ of about 3.15×10^5 gauss centimeters and these would appear to be near the region of 1.8×10^5 gauss centimeters if they were mistaken for protons. It is conceivable that a group of wrongly identified He^3 recoils could thus produce the peak seen in the inelastic proton spectrum.

But although wrongly identified He^3 recoils would have an apparent momentum of about 1.6×10^5 gauss centimeters in their own center of mass system, they would not necessarily have such momentum in the center of mass if transformed as protons. In other words if a group of He^3's were wrongly identified as protons, they would also be incorrectly transformed into the center of mass system as protons.

Fifty-five events, identified as $He^4(p, d)He^3$ were selected at random from the data. The He^3 recoils from these events were transformed into the center of mass system as if they were inelastic protons

to obtain the distribution shown in Fig. 18. There is a peak at $B\rho = 1.4\ 10^5$ gauss cm, and the distribution is such that even if the identification procedure were wrong in this case it could not produce the peak observed in the inelastic proton spectrum.

For completeness it should be mentioned that the pickup deuterons were also transformed into the center of mass system as if they were mistaken for inelastic protons and the result indicated that confusion with the 1.8 proton peak is impossible. Almost all of the incorrectly transformed deuterons had apparent momenta greater than 3×10^5 gauss cm.

There is the possibility that the identification procedure is not only wrong but systematically identifies as inelastic protons only those He^3 recoils that have an apparent momentum of $B\rho = 1.8\ 10^5$ gauss cm. when incorrectly transformed into the center of mass system. Indeed the procedure of identification may systematically select recoils from any two body event for this purpose.

The improbability of such possibilities can be appreciated from a consideration of the auxiliary information used in addition to the basic momentum-energy conservation method of identification. Below is a tabulation of such information for (p, 2p) events.

Of the 58 events identified as (p, 2p):

10 have three ionizing prongs (a characteristic of only this event in He^4 at this energy) of which 7 have one or more prongs identified as protons by $B\rho$ -range and all have two or more of the prongs non-coplanar by 15 degrees or more.

24 of the remaining two prong events have prongs that are non-coplanar by 15 degrees or more (indicating not two body) and in addition 10 of these have one or more prongs identified as protons from $B\rho$ -range.

2 have both prongs identified as protons by $B\rho$ -range.

15 have one of the two prongs identified as protons from $B\rho$ -range.

7 are identified by only the basic method of momentum-energy conservation.

When the (p, 2p) data is divided into various subgroups: the group of events having three visible prongs; the group having non-coplanar prongs; the group in which one or more prongs are identified as protons by Bρ -range; those groups obtained on different days of experiment running time; the group for which all prongs have azimuthal angles less than 45 degrees ($-45^{o} \leq \phi \leq 45^{o}$), then the momenta spectrum of each group is found to have the same general characteristics of that already shown in Fig. 12.

Although it is not expected even if there were confusion with the other inelastic event, $He^{4}(p, pn)He^{3}$, conclusions drawn from the observed proton momentum distribution would not necessarily be invalid since the distribution could indicate properties common to both of these events.

It may be suggested that the 1.8×10^{5} gauss centimeter peak in Fig. 17 is due to an energy level in some contaminating gas, its decay fragments being mistaken for reactions in helium. The possibility of moderate or gross contamination has been considered in the discussion of errors in measurements. If there were slight contamination of the target it would most probably be due to atmospheric oxygen and nitrogen; this is in addition to the known oxygen contamination from the water vapor. Neither of these gases is known to have isolated energy levels in the region that would correspond to the observed proton peak (21 to 23 Mev).* Indeed this statement can be made for any heavy gas, and since there are no common gases that could have contaminated the chamber with anything lighter than carbon (excepting hydrogen which could cause no confusion) it must be concluded that this peak is not due to excitation of a contaminant.

---

*If the group of protons at 1.8×10^{5} gauss centimeters were taken as representative of a level in a heavier gas, then the level indicated would actually be greater than 21 to 23 Mev since more energy is available to a heavier target nucleus.

We shall now consider the possibility that the observed proton momentum distribution could be caused by an excited level in He^4, i.e., $p + He^4 \rightarrow p' + He^{4*} \rightarrow p' + p'' + H^3$. From the momentum and energy conservation appropriate to an excited level process one can show that in general in such a process one should see two peaks in the rest frame of the proton and He^4 system; a sharp peak due to the excitation protons and a broad peak of decay protons. This latter peak is broad because the rest frame of the He^{4*} system is in motion with respect to the rest frame of the primary collision or beam proton-target nucleus system. The broadness and shape of the decay proton peak can be calculated from the kinematics if one assumes a narrow excitation peak.

The momentum spectrum of excitation and decay protons calculated on the assumption of a narrow level at 20.4 Mev is shown in Fig. 19. The value 20.4 Mev was chosen because it gives the spectrum that most closely approaches a fit to the observed data. On the same figure crosses are used to denote the excited level spectrum as it would appear if observed by a histogram, the incremental width of the histogram being equal to that chosen for presentation of the observed data. Notice that the positions of the histogram increments have also been chosen so as to make the excited level spectrum most closely resemble the observed data. The observed data is represented by circles on the same figure.

Even though the optimum conditions for agreement between excited level and observed spectrum have been chosen, the agreement is so poor that one must conclude that the observed spectrum presents no evidence for an energy level in He^4 in this energy range, the range explored extending to slightly more than 23 Mev.

We shall now consider the possibility that the observed spectrum arises from bombardment of a He^4 nucleus in which there are no energy levels, i.e. a process in which the transition matrix is independent of, or a slowly varying function of the final momentum of the beam proton.

The resultant momentum distribution of such a transition is dependent not only on the nature of the transition matrix but also the

density of energy levels, or phase volume, in the final state.

The computation of the unrestricted phase volume available to a proton from this reaction is given in the another paper[15]. The result is

$$V = N\int_{o}^{p_o} p^2(p_o^2 - p^2)^{\frac{1}{2}}\, dp = \frac{N\pi}{16}\, p_o^4 ,$$

where p_o is the maximum proton momentum possible, determined to be 2.05×10^5 gauss cm from the beam energy, and N is an arbitrary constant. N is chosen by equating this phase volume to the area under the momentum histogram representing the experimental results. A plot of the integrand is the differential proton momentum distribution in momentum space to be expected when the transition matrix is nearly constant. The maximum value of the integrand is

$$p_{max} = \sqrt{2/3}\, p_o = 1.67 \times 10^5 \text{ gauss cm}$$

A plot of the integrand is shown in Fig. 20.

It can be seen from this figure that the curve agrees well enough with the experimental points to encourage correcting it for the visibility limitations of the cloud chamber.

In the calculation of this phase volume we ignored the blind regions in the cloud chamber due to scatter angle, momentum and azimuthal limitations, and so we have ignored possible effects these may have on the shape of the phase distribution.

In order to study the effects of the scatter angle and momentum limitations, the region of blindness was mapped on the p - θ plane, where p is laboratory momentum and θ is laboratory scatter angle, by geometrically reconstructing and computing the visibility of the protons and tritons in the cloud chamber. Figure 21 shows two of these regions for protons, one curve demarcates the blind region when the azimuthal limit is assumed to be $\phi \leq |55^o|$ and the other corresponds to $\phi \leq |27.5|$. From these results it is seen that the size of the blind region in θ and p is a very slowly varying function of azimuthal angle.

The region for $\phi \leq |55^o|$ was then transformed into the center of mass system and plotted on a $(p')^2$ vs. cos θ' plane, where p' is

the rest frame momentum. Since $d(p')^2$ and $d(\cos\theta')$ are elements of phase volume for one of the particles, the size of this region compared to the entire plane below the kinematical limit is now a measure of the blind volume. (Fig. 22a and 22b). From these graphs it is found that for (p, 2p) protons the blind volume is only 10.5 % of the total volume available, and it appreciably affects the momentum distribution only in the region of 0.3×10^5 gauss cm. A similar computation for the tritons showed that only 5.6 percent of the triton space was excluded. From this result it was concluded that no significant differences between the observed spectrum and the phase spectrum would arise because of the excluded regions in θ and p due to the presence of the beam.

The azimuthal angle limitation, $-45^\circ \leq \phi \leq 45^\circ$, cannot be so dismissed. It is large - one half of the available geometric volume - and may have strong correlations with momentum. As an example of such correlation consider that two prongs of a three prong event are seen. Conservation of momentum then implies that frequently the azimuthal plane of the third prong will be perpendicular to the mean plane of the first two, and thus the prong will have a high probability of being in an azimuthally excluded region.

Since such correlations could significantly affect the final momentum distribution, it was necessary to introduce suitable functions representing the azimuthal limitations and re-calculate the phase volume integral[15]. By making suitable approximations the result was expressible in terms of elliptic integrals, which when evaluated give the function shown as a solid line in Fig. 17.

This resultant corrected phase volume curve agrees quite well with the observed distribution both in shape and position of maximum.

We have shown that the observed spectrum disagrees with what one would expect from an excited level, and further that it agrees with what one would expect on the assumption of no resonances in the He^4 nucleus in this energy range. For completeness it should be added that if one makes the azimuthal blindness correction to the hypothetical energy level spectrum, the only effect is to make the sloping top of the decay proton peak slightly concave, a correction that does not significantly affect the relation of that spectrum to the observed data.

D. $He^4(p, pn)He^3$ Collisions

Only nine $He^4(p, pn)He^3$ events were seen and identified. This does not imply a cross section extremely small compared to that for $He^4(p, 2p)H^3$. When appropiate allowances are made for the fact that the neutron cannot be seen in a cloud chamber then the cross sections are found to be of the same order of magnitude. Seven of the events had azimuthal angles less than 45^o, and only these are to be counted when comparing the yield with that of other types of events. Because of the smallness of the number of observations no angular distribution is given; only the total number is used for the calculation of a total absolute cross section (Table I, page 35).

No other events were observed. The fact that no positively identifiable $He^4(p, p\gamma)He^4$ events were seen has already been discussed in detail in the section on analysis. This result implies that there is no excited He^4 level in this energy region that decays principally by γ-decay rather than heavy particle emission, and either the inverse photo-disintegration process suggested by Flowers and Mandl[8] has too small a cross section to contribute in this energy region or the threshold for it is too high.

E. Comparative Cross Sections

Table I below summarizes the yields of the various reactions. Column three lists the number of events seen, identified and satisfying the condition $\phi \leq \pm 45^o$. Column four lists the factors that correspond to the different probabilities of being seen due to the azimuthal limitations on visibility, (computed in reference[15]) and column six those factors arising from the scatter angle limitations on visibility. The normalization of the elastic proton-helium events to the results of Cork[11] assigns total cross section values to the different reactions in column eight. These total cross section values are obtained by assuming an isotropic center of mass angular distribution for the inelastic three body reactions, an assumption borne out by such experimental evidence as was obtainable from the p, 2p reaction. Column two lists the total number of each type of event seen with no restrictions on azimuthal angle ϕ.

TABLE I

Type of Event	Number Observed	Number Observed, $\phi \leq \pm 34^{o}$	Azimuthal (ϕ) Visibility (Per Event)	Number Observed, Azimuthally Corrected	Polar Angle (θ) Visibility	Number Observed, Corrected For Polar Angle Visibility	Total Cross Section in Millibarns
Elastic p-α		2,125	1/2	4,250			*
$He^4(p, D)He^3$	185	167	1/2	334			**
$He^4(p, pn)He^3$	9	7	1/4	24	0.527 ±.032	53.1±30.7	4.8±3.0
$He^4(p, 2p)H^3$	58	40	1/2	80	0.813 ±.036	98.3±14.4	8.86±1.30
$He^4(p, p\gamma)He^4$	Not observed						$0 + 2$ $- 0$

* Differential cross section given in Fig. 7

** Differential cross section given in Fig. 10.

Notice in the above table that the polar angle corrections and the azimuthal angle corrections were handled as separate factors, i.e. possible correlations between the two effects were ignored. This was justified by simultaneously introducing both the azimuthal and polar angle projection terms into the phase volume integral and carrying out the intergration graphically. This was done for the $He^4(p, n)He^3$ type of event, a type of event for which the correction factors were largest. The result so obtained agreed with the result obtained by considering the polar angle correction as a separate and independent factor to within three percent. It was then assumed that the separate factor correction procedure was also allowable for $He^4(p, 2p)H^3$ events.

IV. SUMMARY

When He^4 is bombarded with 28 Mev protons the dominant reaction is elastic scattering which exhibits a strong peak in the forward direction and a slight rise in the backward direction indicative of exchange type interaction. The dominant inelastic reaction is the inverse Butler or pickup deuteron process. Its angular distribution agrees with Butler's theory except at large scatter angles ($\theta' > 90^\circ$).

The two remaining inelastic reactions observed, the $He^4(p, 2p)H^3$ and $He^4(p, pn)He^3$ processes, have cross sections of 8.86 ±1.30 millibarns and 4.8 ±3.0 millibarns, respectively. These are an order of magnitude or more smaller than the cross sections of the dominant processes.

Of the remaining possible reactions: (p, pd), (p, n2p) (p, pγ), only the last is energetically possible at the beam energy used. It was not observed. This indicates no evidence for an excited level in He^4 in the energy region of 0 to 23 Mev that decays principally by γ-ray emission, and also indicates that either the inverse photodisintegration process suggested by Flowers and Mandl[8] has too small a cross section in this energy region to contribute or that this energy region lies below the threshold for the process.

The rest frame momentum spectrum of protons from the $He^4(p, 2p)H^3$ reaction presents no evidence of an excited level in He^4 in an energy region extending to slightly more than 28.0 Mev, the observed spectrum agreeing quite well with the spectrum expected on the assumption of no levels in He^4.

ACKNOWLEDGMENTS

The author wishes to express his sincere gratitude to Professor Wilson Powell and Dr. T. C. Merkle for their helpful advice and constant encouragement throughout the investigation. The cooperation of many members of the cloud chamber group is also acknowledged with pleasure, especially that of John Need and Oscar Kolar who assisted during running time and who helped to prepare the cloud chamber.

The author is indebted to Mr. Edward Vaughn for many hours of theoretical discussion and interpretation of the data.

This work was supported by the Atomic Energy Commission.

APPENDIXES

A. Kinematical Relations

In the case of elastic p - α scattering the following useful relations can be verified readily by conserving momentum and energy. Primes always indicate quantities referred to the center of mass system.

$$v' = \frac{m_p}{m_\alpha} v'_p \approx 1/4\, v'_p. \tag{1}$$

$$v_{cm} = \frac{m_p v_o}{m_p + m_\alpha} \approx \frac{v_o}{5} \tag{2}$$

$$v_{cm} \approx v'_\alpha, \tag{3}$$

where v_{cm} is the velocity of the center of mass system and v_o the velocity of the beam protons.

$$E_\alpha \approx \frac{16}{25} E_o \cos^2 \theta_\alpha, \tag{4}$$

where E_o is the beam energy.

$$\theta'_p = 180^o - 2\theta_\alpha. \tag{5}$$

$$\theta'_\alpha = 2\theta_\alpha. \tag{6}$$

The following center of mass transformations are valid in general. From the law of sines, (refer to Fig. 23)

$$\sin(\theta' - \theta) = \frac{v_{cm}}{v_p} \sin\theta'. \tag{7}$$

A similar expression was used to transform momenta into the center of mass system:

$$p' = \frac{\sin}{\sin\theta'} p, \tag{8}$$

which can also be written

$$\sin \theta' = \frac{v}{v'} \sin \theta. \tag{9}$$

Further modification, using the law of cosines, gives

$$\sin \theta' = \frac{(v'^2 + v_{cm}^2 - 2v'v_{cm}\cos \theta)^{\frac{1}{2}} \sin \theta.}{v'} \tag{10}$$

For a two body problem all of the quantities, except θ, on the right side of (10) can be expressed in terms of E_o. Thus, for deuterons for the reaction $He^4(p, D)He^3$,

$$v'_D = \left\{ \frac{m_{He^3}}{m_{He^3} + m_D} \left(\frac{m_{He^4}}{m_{He^4} + m_p} E_o - Q \right) \right\}^{\frac{1}{2}} \left\{ \frac{m_D}{2m_p} \right\}^{\frac{1}{2}} \tag{11}$$

and

$$v_{cm} = \frac{m_p}{m_p + m_{He^4}} \left(\frac{2E_o}{m_p} \right)^{\frac{1}{2}} \tag{12}$$

can be put into the right hand side of (10). Expressions similar to (11) and (12) hold for the recoil He^3 particles. These expressions together with

$$\theta'_D = 180^o - \theta'_{He^3} \tag{13}$$

enable one to construct a family of curves, $\theta_D = \theta_D (\theta_{He^3}, E_o)$.

Initially the analysis was attemped as follows:

1. Find E_o from $\theta_D = \theta_D (\theta_{He^3}, E_o)$.
2. Use E_o in equations (11) and (12) to obtain θ'_D from (10).

This was achieved in two steps using two graphs of families of curves, E_o taken as a parameter.

Unfortunately this procedure was found to compound the errors in θ. The precedure finally adopted was:

1. Find θ'_D from (10) with the aid of (11) and (12), taking E_o as an

average determined by independent measurements (E_o = 27.9 Mev).

2. Find θ'_{He^3} from equations similar to (10), (11) and (12); then find $\theta'_D = 180^o - \theta'_{He^3}$.

3. Average results of step 1. and 2.

All other inelastic events were analyzed by means of equations (8) and (9), where the momenta and velocities were obtained from $B\rho/e$ and $B\rho/em$, respectively.

The elastic scattering was analyzed in terms of $\Delta = \theta_p + \theta_{He^4}$, a quantity independent of initial beam direction. Use of Δ greatly expedited the actual measurement of the tracks, although it made the analysis more complex. From Fig. 23 we see that

$$\delta = \pi - \theta_p - 2\theta_\alpha. \tag{14}$$

From the law of sines, $\frac{\sin\theta_p}{\frac{1}{4}} = \frac{\sin\delta}{1} \sin(\pi - (\theta_p + 2\theta_\alpha)) = \sin(\theta_p + 2\theta_\alpha) = \sin(2\Delta - \theta_p)$, or $\frac{1}{4}\sin\theta_p = \sin 2\Delta \cos\theta_p - \cos 2\Delta \sin\theta_p$. Division by $\cos\theta_p$ and rearrangement gives

$$\tan\theta_p = \frac{\sin 2\Delta}{\frac{1}{4} + \cos 2\Delta}. \tag{15}$$

If exact masses are used than (14) remains valid but (15) becomes:

$$\tan\theta_p = \frac{\sin 2\Delta}{0.2518 + \cos 2\Delta}. \tag{15'}$$

Δ if given from the original measurements by

$$\cos\Delta = \cos\Delta' \cos\alpha_2 \cos\alpha_2 - \sin\alpha_1 \sin\alpha_2, \tag{16}$$

where $\Delta' = \beta_p + \beta_\alpha$. Equation (15'), together with $\Delta = \theta_p + \theta_\alpha$ and equation (5), allows one to construct graphs relating Δ to θ_p, and Δ to θ'_p.

The majority of elastic alpha recoils stopped in the chamber. In this case only R (range) was measured, range energy curves were used to obtain E_α from R, and then Δ from

$$\sin \Delta = \frac{1 - \frac{25}{16}\frac{E_a}{E_o}}{1 - \frac{E_a}{E_o}} \qquad (17)$$

allowed the analysis to be carried out as before.

To derive (17) one first finds from Fig. 23 and the law of sines

$$\frac{\sin \theta_a}{v_p} = \frac{\sin \Delta}{5}, \text{ or}$$

$$\sin \Delta = \frac{5 \sin \theta_a}{\left(\frac{2(E_o - E_a)}{m_p}\right)^{\frac{1}{2}}} \qquad (18)$$

where here m_p is in units of $m_p = \frac{2E_o}{25}$. In the same units the square root of equation (4) becomes

$$\cos \theta_a = \frac{1}{2}\sqrt{\frac{E_a}{2m}}. \qquad (4')$$

Equation (4') also can be derived directly from the figure by the law of cosines. (4') and (18) immediately give (17).

B. Definitions of Quantities Measured.

In Fig. 8

$\overline{OT}$ is the direction of the beam

$\overline{OR}$ is the direction of a prong of an event

$\overline{OS}$ is the projection of OR on the horizontal plane

$\overline{OT}$ is the projection of OR in the direction of the beam

(In the case of a two body event OTR defines the plane of the event)

α is the dip angle, the angle of inclination to the horizontal plane

θ is the scatter angle, the angle between prong and beam direction

β is the beam angle, the horizontal projection of θ

ϕ is the azimuthal angle, the angle between the plane of the event and the horizontal plane.

From the figure one derives: $\overline{OR} \cos \alpha \cos \beta = \overline{OR} \cos \theta$, or

$$\cos \theta = \cos \alpha \cos \beta; \tag{1}$$

$\overline{OR} \sin \theta \sin \phi = \overline{OR} \sin \alpha$, or

$$\sin \phi = \frac{\sin \alpha}{\sin \theta}; \text{ similarly} \tag{2}$$

$$\sin \beta = \sin \theta \cos \phi. \tag{3}$$

Let AB be a line perpendicular to $\overline{OR}$ and wholly contained in the horizontal plane defined by OTS. Then the plane containing the line $\overline{OR}$ and all points on the line AB is called the slant plane. This is the plane in which the radius of curvature is measured.

C. Slant Plane Reprojection and Azimuthal Reprojection.

We shall define two types of reprojection, slant plane reprojection and azimuthal reprojection. In slant plane reprojection one reprojects the track onto a plane defined by the track and a horizontal line perpendicular to the track, and measures the dip angle α, the angle of the reprojection plane to the horizontal, and the beam angle β, where β is the angle between the horizontal projection of the track and the beam direction (see Fig. 8). The scatter angle θ is obtained from $\cos\theta = \cos\alpha \cos\beta$. In azimuthal reprojection one reprojects the track onto a plane defined by the track and the beam. Here one can measure the scatter angle θ directly.

When the tracks are curved into helical paths by a magnetic field, errors in measurement are introduced that are inherent to the method of reprojection. We shall now consider these errors.

Fig. 24a shows a reprojected straight track and the same track curved by a magnetic field. Conservation of energy and momentum requires that their ranges and vertical rise be equal. From the figure we have $\sin\alpha = x/R$ and $\sin\alpha' = x'/r = \frac{x}{2\rho \sin\frac{R}{2\rho}}$,

therefore $\frac{\sin\alpha' - \sin\alpha}{\sin\alpha} = \frac{R}{2\rho \sin\frac{R}{2\rho}} - 1 \approx \frac{2\rho}{R}\left(\frac{1}{\frac{R}{2\rho} - \frac{R^3}{3!8^3}}\right) - 1$

$\approx R^2/24^2$. This is a small quantity seldom exceeding 1/2%.
By diffentiating $\cos\theta = \cos\alpha \cos\beta$ and dividing the result by $\cos\theta$

we find $\frac{d(\sin\theta)}{\sin\theta} = \frac{d(\sin\alpha)}{\sin\alpha} = \frac{\sin\alpha' - \sin\alpha}{\sin\alpha}$ since β is held constant. Therefore the percentage error in $\sin\theta$ is also $(R/24)^2$.

In the case of azimuthal reprojection Fig. 24b is appropriate and we see that if $\sin\phi = x/R \sin\theta$, then $\sin\phi' \approx \frac{x}{R \sin(\theta + \frac{R}{2\rho})}$,

so that $\frac{\sin\phi' - \sin\phi}{\sin\phi} = \frac{\sin\theta}{\sin(\theta + \frac{R}{2\rho})} - 1 \approx \frac{-1}{1 + \frac{2\rho}{R}\tan\theta}$

If we differentiate $\sin\theta = \frac{\sin\alpha}{\sin\phi}$ and divide the result by

$\sin\theta$ we find $\frac{d\sin\theta}{\sin\theta} = \frac{d\sin\alpha}{\sin\alpha} - \frac{d\sin\phi}{\sin\phi}$. The error in $\sin\alpha$ will be the same as in slant plane reprojection, therefore

$$\frac{d\sin\theta}{\sin\theta} \approx \frac{R^2}{24\rho^2} + \frac{1}{(1 + \frac{2\rho}{R}\tan\theta)}, \quad \frac{2\rho}{R} << 1 .$$

We see that for small θ the error in θ can become rather large due to the second term on the right hand side of the above expression. In practice it was found that for many p - α elastic scatters the error was 8^{o} or more. Furthermore the reprojection was hindered by the fact that the two prongs of an elastic scatter no longer define an azimuthal plane for the event, their different curvatures having carried them different distances out of the true azimuthal plane of the event. Because of these difficulties it is advisable to use slant plane reprojection.

D. Sample Analysis of Two Events

1. Event No. 5709A. It was recorded that this was a two prong event with one prong on either side of the beam. The following information was available:

	prong No. 1	prong No. 2
Dip angle	5.7^{o}	7.8^{o}
Beam angle (corrected for position of origin)	34.8^{o}	39.8^{o}
Slant radius of curvature, ρ_s	70 cm.	25 cm.
Scatter angle	35.2^{o}	40.5^{o}
$B\rho$ (in gauss centimeters)	5.43×10^5	2.44×10^5
Range		9.6 cm.
Estimated ionization (relative to minimum ionization)	100	450
Azimuthal angle	9.9^{o}	12.1^{o}

The values of ϕ in the last row of the table indicate coplanarity, i.e. a $He^4(p, d)He^3$ or $He^4(p, p\gamma)He^4$ event since the only other possible two body event, elastic scattering, has already been eliminated.*

The actual analysis is shown below. Line three records the possible types of particles, their energies, (corresponding to the observed $B\rho$) and line four their ionizations. Those particles having impossibly high kinetic energies have been struck out. Line five records the observed estimated ionization, and those values in line three that agree with it are underlined.

The values of $B\rho$ and range identify the second prong as either a deuteron or He^3. Line six records the kinetic energy a deuteron or He^3 would have if it had the range observed. Lines seven and eight are similar to lines four and five. Line nine records $B\rho$ as determined from range.

At this point it can be seen that there are only four combinations: d-d; d-He^3; t-d; t-He^3; of which only the second is possible.

On lines ten to twelve the momentum is balanced transversely as if the event were a d-He^3 type. Descrepancies up to $\delta = 0.50$

* Notice, for example, that $\theta_1 + \theta_2 = 35.2 + 40.5 = 75.7 = \Delta$, but $\Delta \geq 90^{o}$ for elastic scatters.

were considered to indicate agreement. Next the momentum is balanced longitudinally and the percentage differences indicated on line sixteen. Percentage differences up to eight percent are considered to indicate agreement. On lines nineteen to twenty-two the kinetic energies are added and compared with the allowed kinetic energies. The d-d-(p) possibility is cancelled out because only two of the three possible prongs already have more than an allowable kinetic energy. This last statement, together with the observed coplanarity, definitely eliminates the d-d-(p) possibility, and it is consistent with the transverse and longitudinal conservation of momentum.

Analysis

1. ϕ: $+9.9^{o}$, -12.1^{o}; indicates coplanarity.
2.
3. 1. from Bρ: 15.4p; 8.1H^2; 5.4H^3; 21.3He^3
4. expected ion. 16 49 100 122
5. observed ion. 100
6. 2. BρR → D, He^3; from R; 1.1 H^2; 3.0 He^3
7. 198 580
8. 450
9. Bρ from R: 2.16H^2; 2.18 He^3
10. transverse momentum: 5.43 sin 35.2 = 4.88 sin 40.5,
11. 3.13 = 3.17
12. δ = 0.04
13.
14. longitudinal: 5.43 cos 35.2 + 4.88 cos 40.5 = 7.70
15. 8.15 = 7.70
16. $\frac{8.15 - 7.70}{7.70}$ = 5.8% error.
17.
18.
19. D-He^3 7.0
20. 3.9
21. 10.9
22. cp. 9.7 Mev

2. Event No. 5769A is an example of one of the more difficult to analyze. The analysis starts as in the preceding example. The notation Bρ >R → p, D, He^3 on line six indicates that although the particle did not stop in the chamber, the track was longer than that for a triton of this Bρ. On lines ten to twenty the discrepancies in transverse horizontal, transverse vertical, and longitudinal momentum conservation are computed. Then the equations on lines twenty-two, twenty-three and twenty-four specify the momentum conditions that the third

unseen particle must satisfy.

From the momentum conditions ϕ, θ and $B\rho$ are computed for the unseen particle. The energies associated with the different types of possible particles having such $B\rho$ are then combined with the different possibilities listed on lines three and six. This is done on lines thirty-three to thirty-six. The results are compared with the allowable energies listed on line thirty-seven, and impossible energy values are cancelled out.

It is seen that this procedure establishes the type of event as $He^4(p, 2p)H^3$, but leaves the identity of the visible prongs uncertain: p + p + (t), or t + p + (p). The latter is chosen on the basis of ionization. The location of the unseen particle is summarized on lines forty-one to forty-three together with a few remarks explaining why the particle was not seen.

The analysis still is not complete because the possibility He^3 + p + (n) has not been eliminated. Because the momentum equations are different for a doubly charged particle the momentum analysis has to be repeated. This is done on lines forty-seven to seventy. It is shown that if the unseen particle is a neutron, then momentum balance necessitates more than the allowed kinetic energy for that type of reaction.

Analysis

1. ϕ: + 49.2°; - 3.4°, not coplanar.
2.
3. 1. from $B\rho$: 2.9p; 1.5D; 1.0T; 3.9He^3; 2.9He^4
4. 63 165 260 515 600
5. Obs. 225
6. 2 . $B\rho$ > R→ p, D. He^3; from $B\rho$: 5.5p; 2.8D; 7.4He^3
7. 38 123 295
8. Obs. 25
9.
10. transverse: 2.45 sin 37.1 cos 49.2 = 3.40 sin 24.1 cos 3.4
11. (horizontal) 0.97 = 1.39
12. δ_H = 0.42
13. vertical: 1.12 = 0.08,
14. δ_v = 1.04
15.
16. long. bal. 1.96 + 3.10 = 7.70
17. 1.96 - 5.06
18. 5.06 2.64
19.

$\delta_e = 2.64$

$B\rho \cos\theta = 264$

$B\rho \sin\theta \cos\phi = 0.42$

$B\rho \sin\theta \sin\phi = 1.04$

$\tan\phi = \frac{1.04}{0.42}$, or $\phi = 68.0^\circ$

$\tan\theta \cos 68.0 = \frac{0.42}{2.64}$, or $\theta = 23.0^\circ$

$B\rho \cos 23.0 = 2.64$, $B\rho = 2.87$

from $B\rho = 3.18$: 4.8p; 2.4D; 1.6T; 6.3He^3

	pp(T)	Tp(p)
	2.9	1.0
	5.5	5.5
	1.4	4.0
	9.8	10.5
cp.	8.4	8.4

T-p-(p) preferred by ionization comparison.

origin, s = 8.2 cm
$\theta = 20.6^\circ$
$\phi = 68.0^\circ$

too steep; also, if seen, probably would be considered as part of spray from the thin window.

He^3 + p + (n) possibility:

trans: $1.94 = 1.39$

$\delta_H = 0.45$

vert.: $2.24 = 0.08$, $\delta_v = 2.16$

long: $3.92 + 3.10 = 7.70$

$3.92 - 7.02$

$7.02 \quad 0.68 = \delta_\ell$

$B\rho \cos\theta = 0.68$

$B\rho \sin\theta \cos\phi = 0.45$

$B\rho \sin\theta \sin\phi = 2.16$

$\tan\phi = \frac{2.16}{0.45}$, or $\phi = 78.2^\circ$

$\tan\theta \cos 78.2 = \frac{0.45}{0.68}$, $\theta = 72.8^\circ$

$B\rho \cos 72.8^\circ = 0.68$, $B\rho = 2.30$

$B\rho = 2.30 \rightarrow 2.2$ Mev neutron.

He^3 + p + (n)	3.9
	5.5
	2.2
	11.6 Mev
	7.5 Mev allowed.

BIBLIOGRAPHY

1. E. Feenberg, Phys. Rev. 49, 328 (1936)
2. H. A. Bethe and R. F. Bacher, Rev. Mod. Phys. 8, 147 (1936)
3. H. R. Crane, L. A. Delasso, W. A. Fowler and C. C. Lauritsen, Phys. Rev. 48, 100, 102, 125 (1935)
4. L. D. P. King and L. Goldstein, Phys. Rev. 75, 1366 (1949)
5. J. H. Coon and R. A. Nobles, Phys. Rev. 75, 1358 (1949)
6. R. Batchelor, J. S. Epstein, B. H. Flowers and A. Whittaker, Nature 163, 211 (1949)
7. H. V. Argo, H. T. Gittings, A. Hemmindinger, G. A. Jarvis and R. F. Tascheck, Phys. Rev. 78, 691 (1950)
8. B. H. Flowers and F. Mandl, Proc. Roy. Soc. (London) A 206, 131 (1951)
9. J. Benvenisti, "Inelastic Events Induced by 32 Mev Protons on Helium" (thesis), University of California Radiation Laboratory Report No. UCRL-1689, March 1952.
10. Brueckner, Hartsough, Hayward and W. Powell, Phys. Rev. 75, 555 (1949)
11. B. Cork, "The Elastic Scattering of Protons from Helium 4", University of California Radiation Laboratory Report No. UCRL-1673, February 1952.
12. S. T. Butler, Proc. Roy. Soc. (London) A 208, 559-79 (1951)
13. G. A. Jarvis, A. Hemmendinger, H. V. Argo and R. F. Taschek, Phys. Rev. 79, 929 (1950)
14. H. A. Bethe, Phys. Rev. 70, 821 (1946)
15. A report on the effects of limited visibility on momenta spectra obtained by the cloud chamber technique will be published in the near future by E. U. Vaughn of this laboratory.

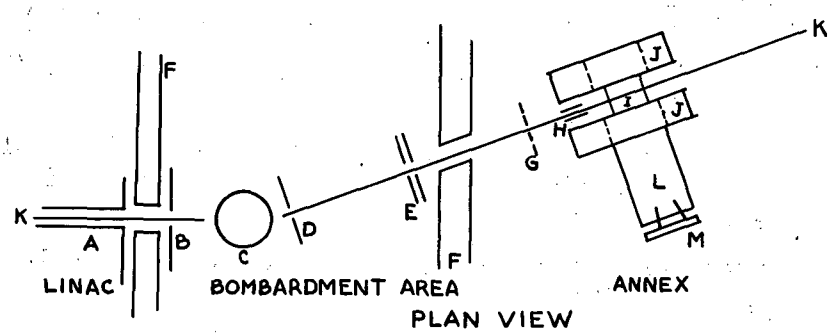

PLAN VIEW

A HIGH ENERGY END OF LINAC
B 4 JAW COLLIMATOR
C STEERING MAGNET
D PRIMARY COLLIMATOR
E SECONDARY COLLIMATOR AND CLIPPER
F WALLS OF BUILDING
G THIN WINDOW AT END OF BEAM TUBE
H ION CHAMBER
I CLOUD CHAMBER
J HELMHOLZ COILS
K PROTON BEAM
L CAMERA TUBE
M STEREOSCOPIC CAMERA

MU-8025

Fig. 1 Plan View of the Experimental Geometry.

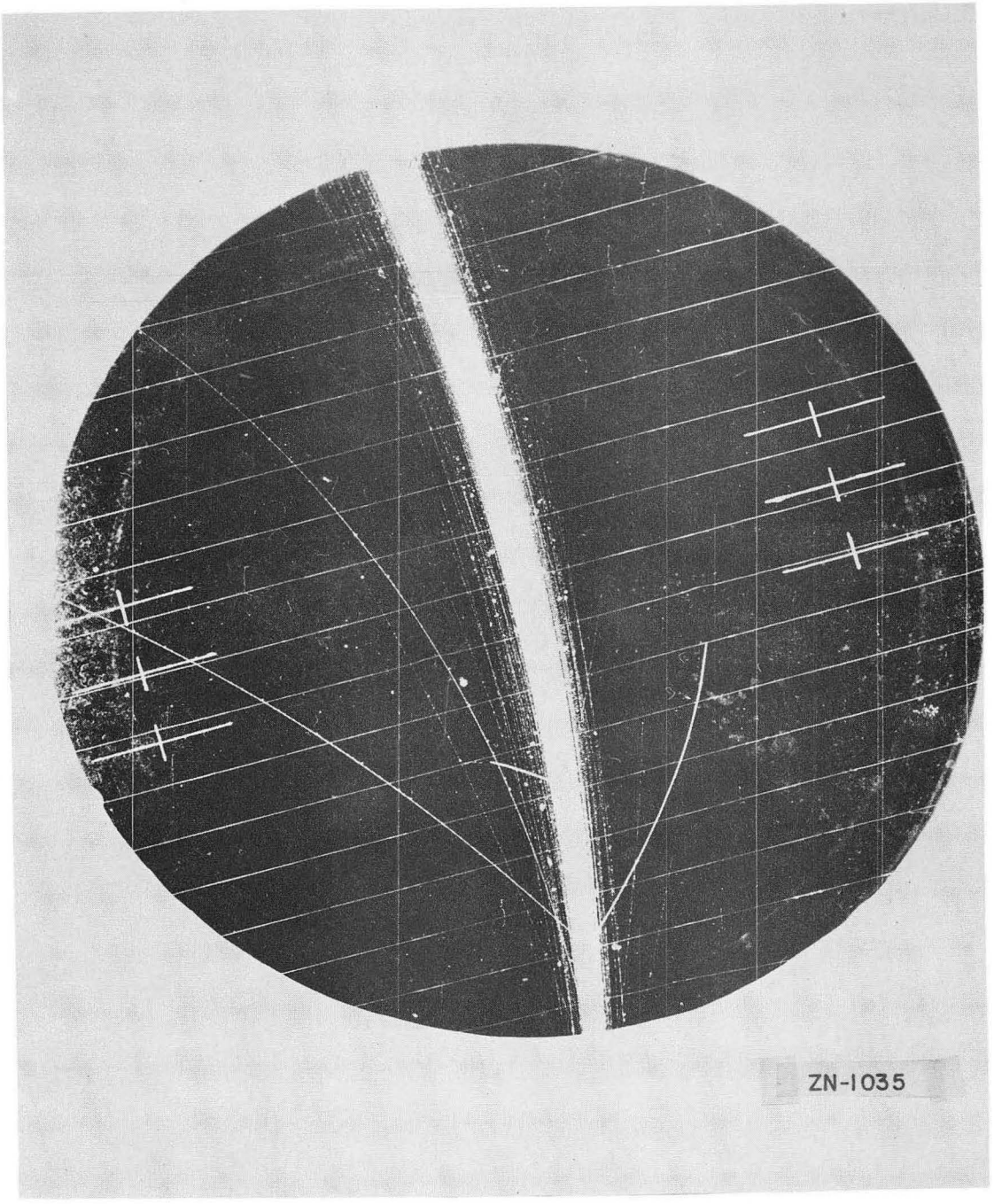

Fig. 2 Enlargement of an Entire Cloud Chamber Photograph.

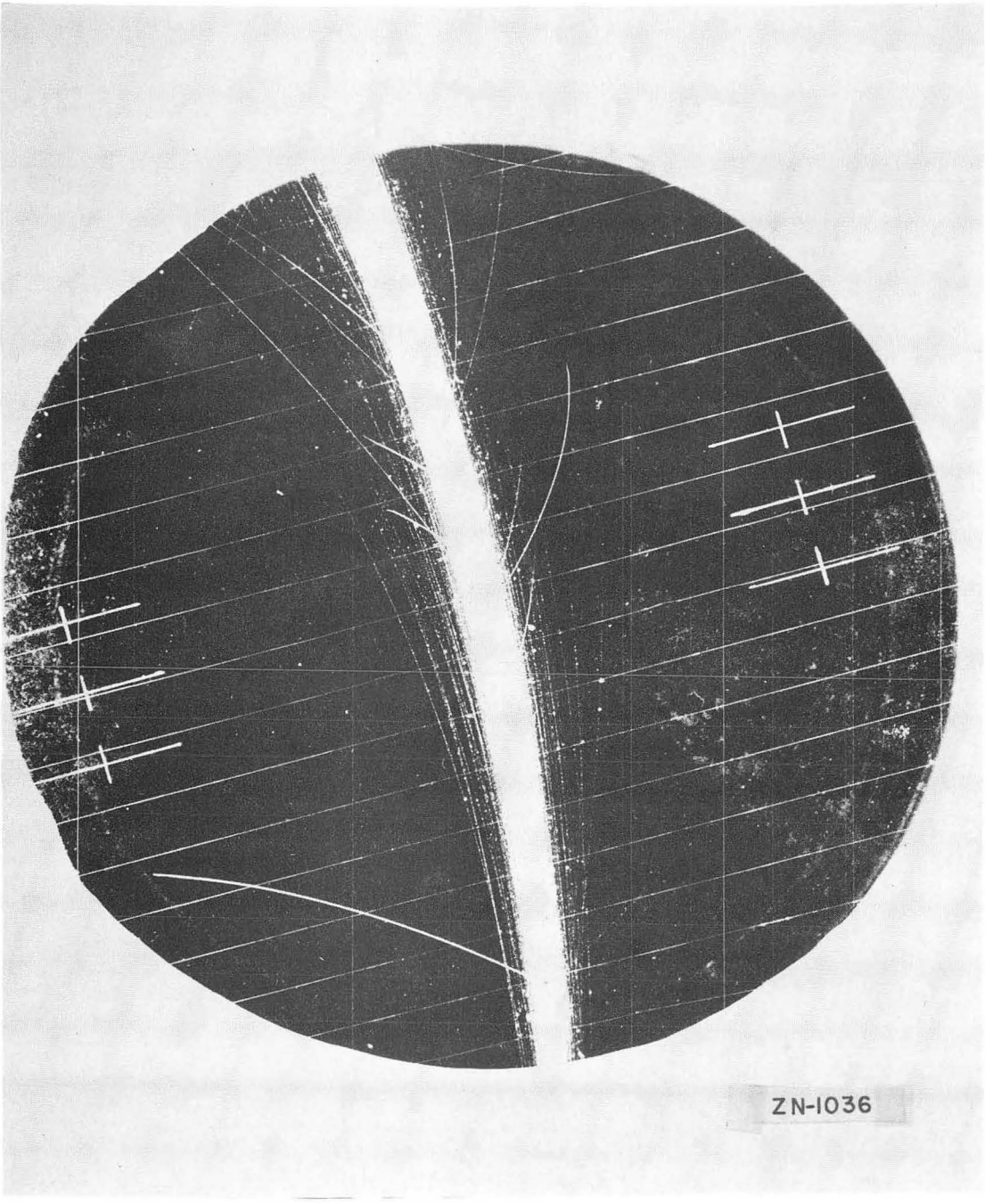

Fig. 3 Enlargment of a Cloud Chamber Photograph Showing a Wide Angle Elastic Scatter at the Bottom and a Cluster of Several Events at the Top. All of the Prongs in the Cluster that Satisfied the Condition $\phi \leq 45^{\circ}$ were Identifiable.

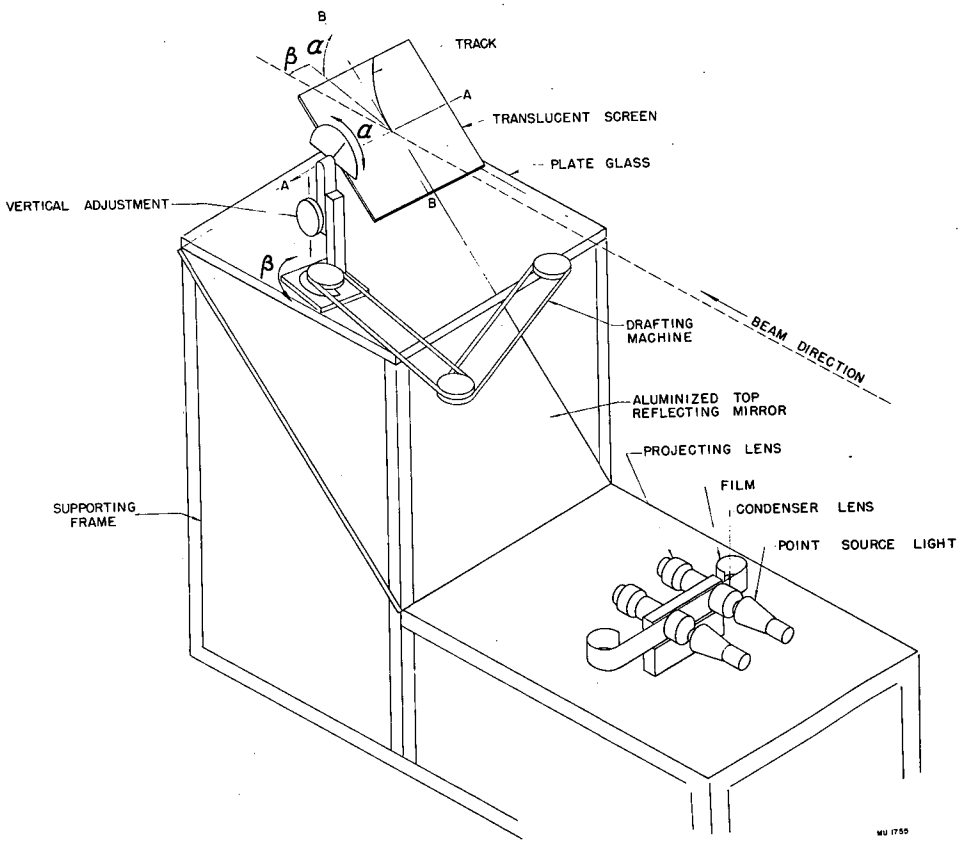

Fig. 4 Isometric Projection of Reprojection Apparatus.

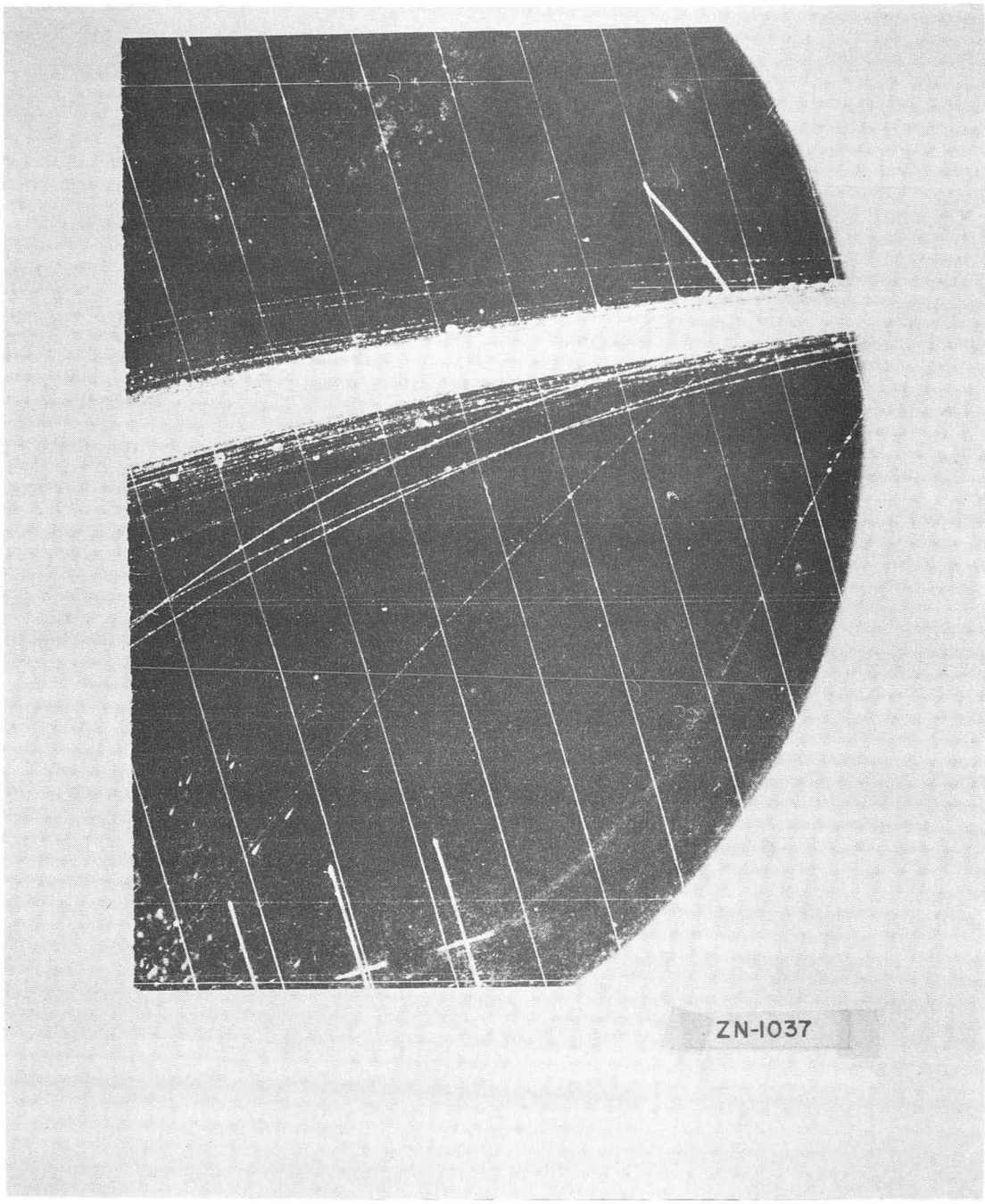

Fig. 5 Enlargement of a Cloud Chamber Photograph Showing an Elastic Proton-Helium Scatter. The Short Heavily Ionizing Recoil Alpha Particle Stops in the Gas of the Chamber; the Scattered Proton Traverses the Entire Lower Portion of the Picture at an Angle of 35° to the Beam.

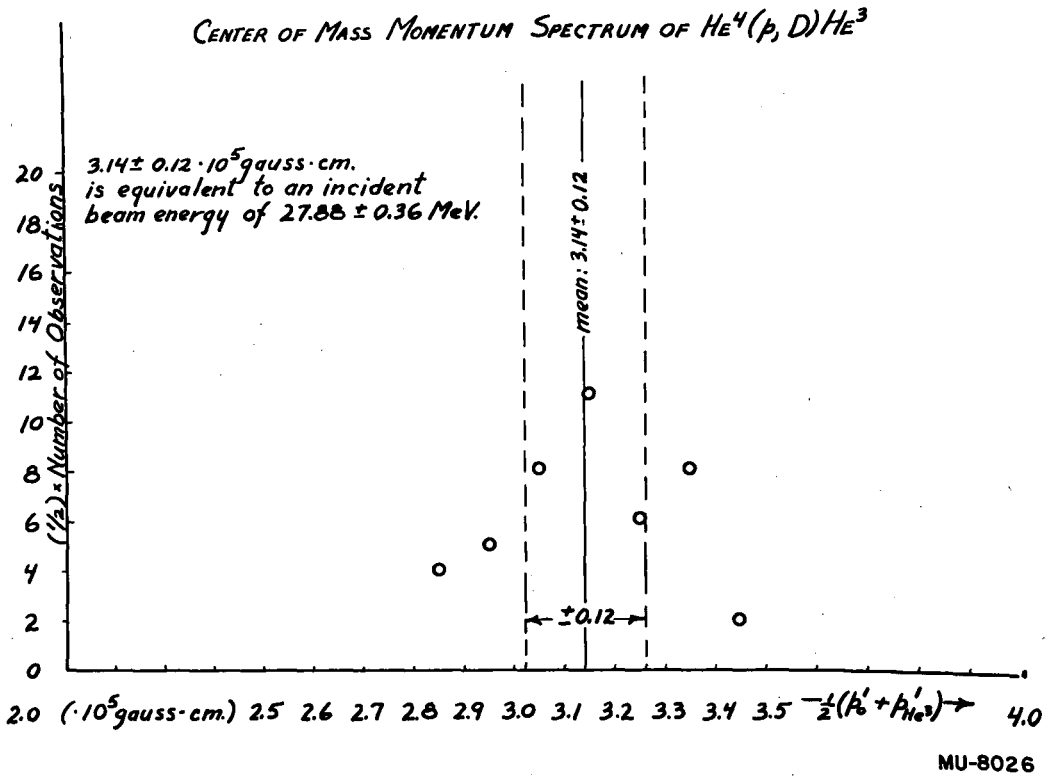

Fig. 6 Center of Mass Momentum Distribution of He^4 (p, D) He^3 Reactions.

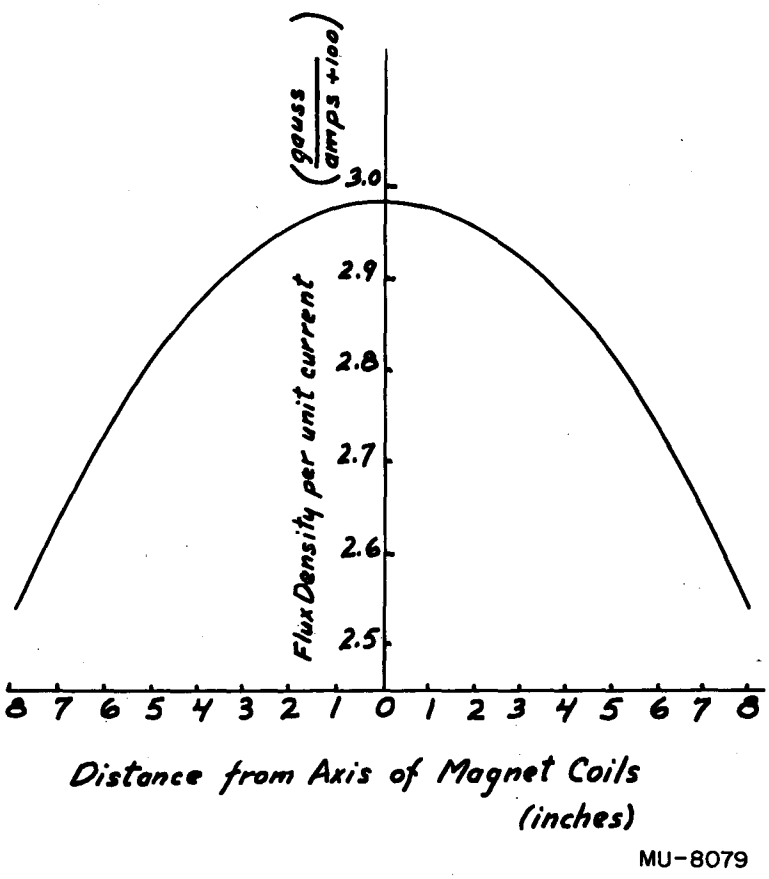

Fig. 7 Flux Density as a Function of Radius for the 16 inch Cloud Chamber Magnet.

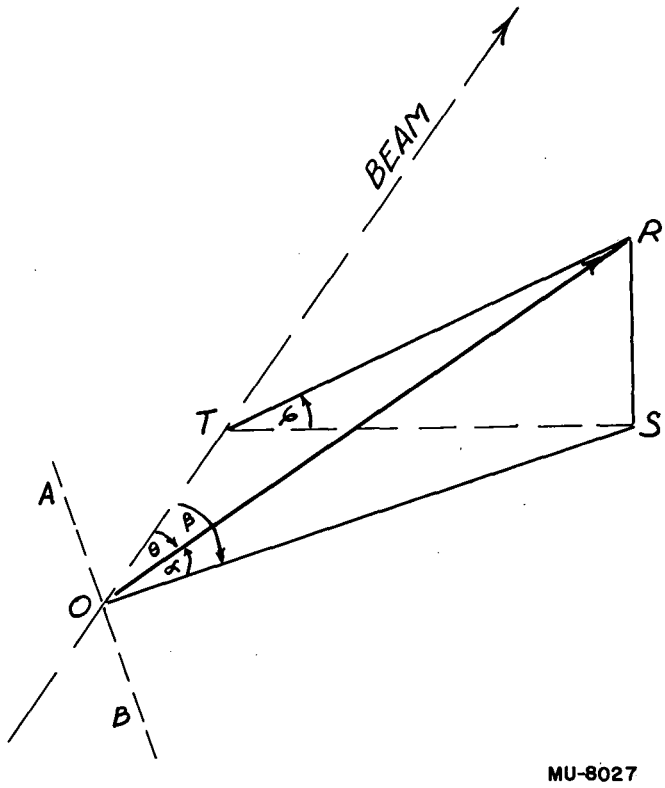

Fig. 8 Definition of Angular Coordinates Used in Cloud Chamber Measurements.

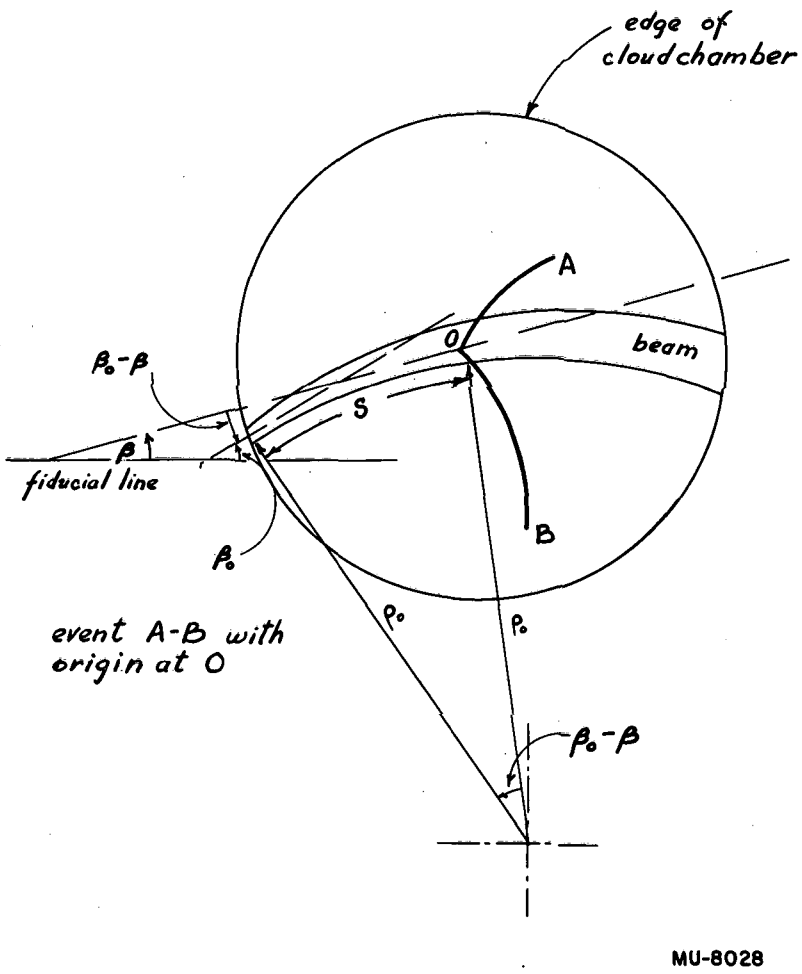

Fig. 9 Schematic Diagram of Beam Curvature and the Coordinates Used to Measure it.

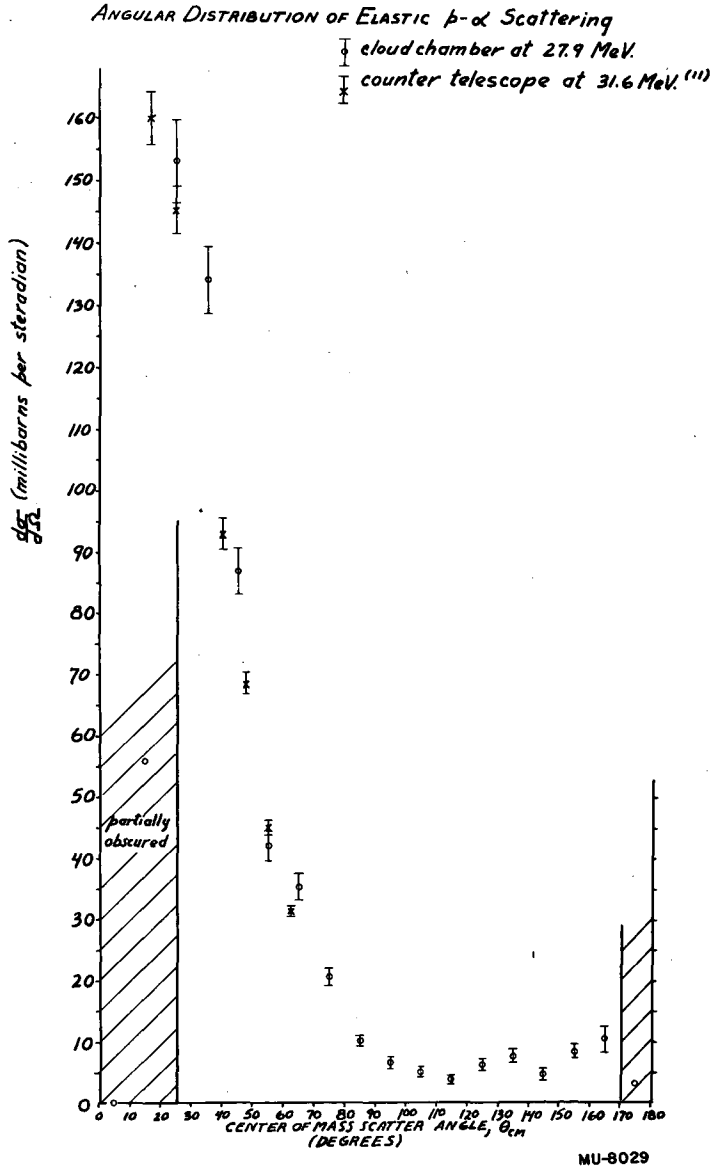

Fig. 10 Elastic Proton-Helium Center of Mass Angular Distribution, Number of Protons in Intervals of 10^{o} of Center of Mass Scatter Angle.

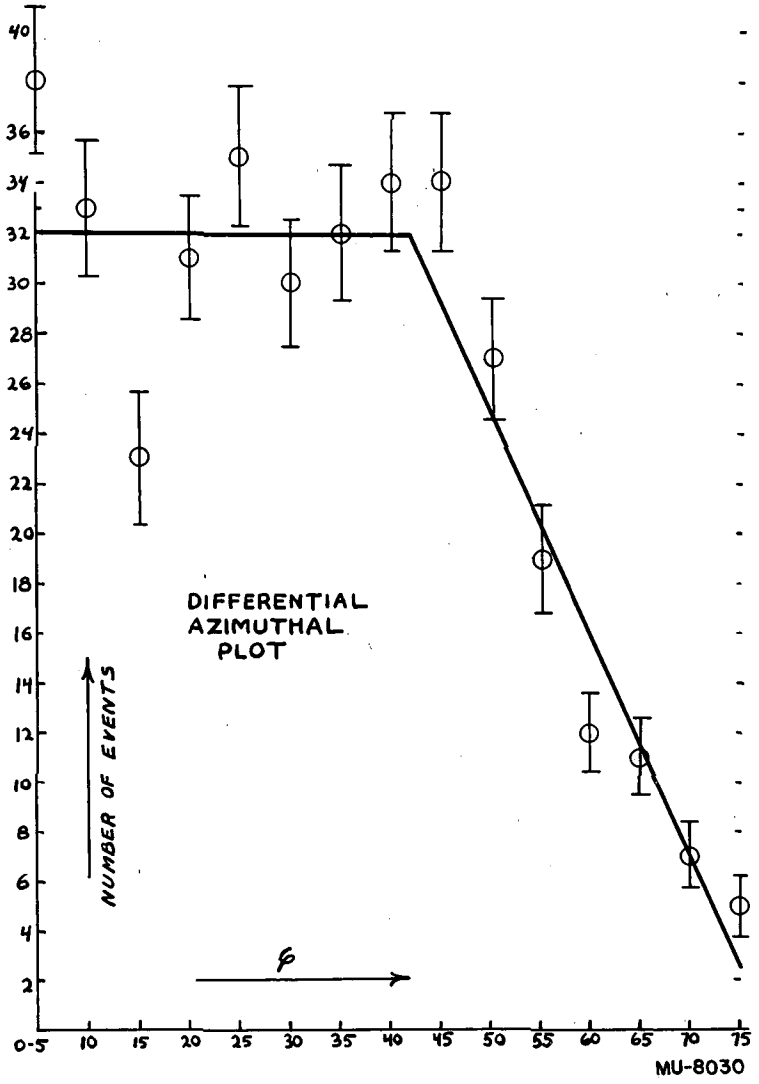

Fig. 11 Differential Azimuthal Plot Showing Number of Protons from Proton-Helium Elastic Scatters in 5^{o} Intervals of Azimuth.

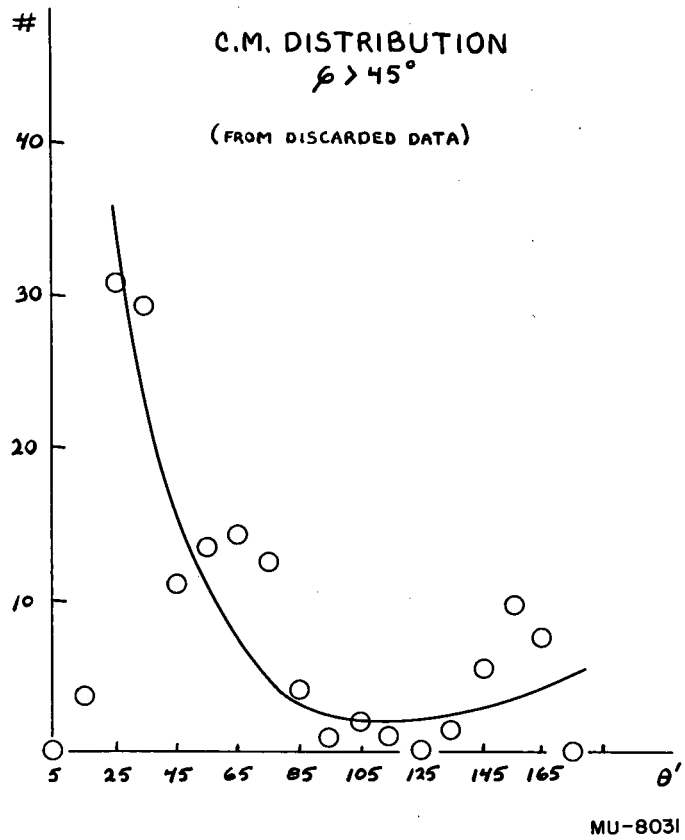

Fig. 12 Elastic Proton-Helium Center of Mass Angular Distribution from Discarded Data.

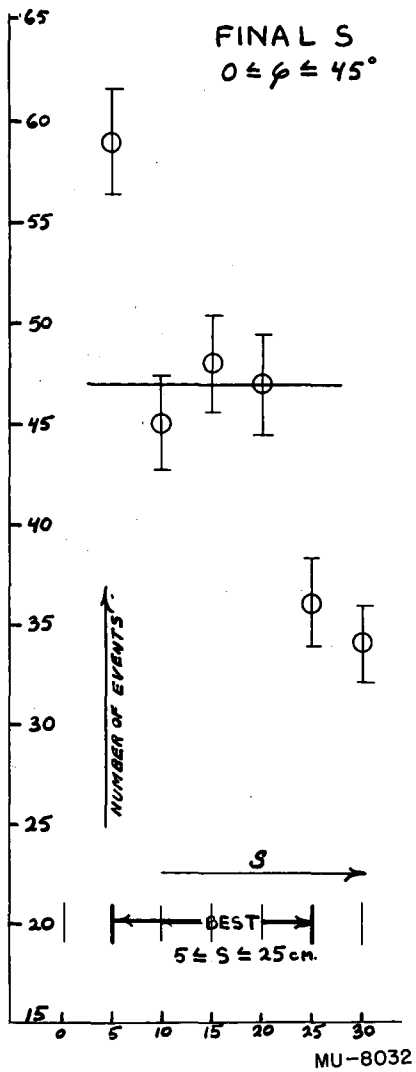

Fig. 13 Number of Events in 5 cm Intervals Along the Beam.

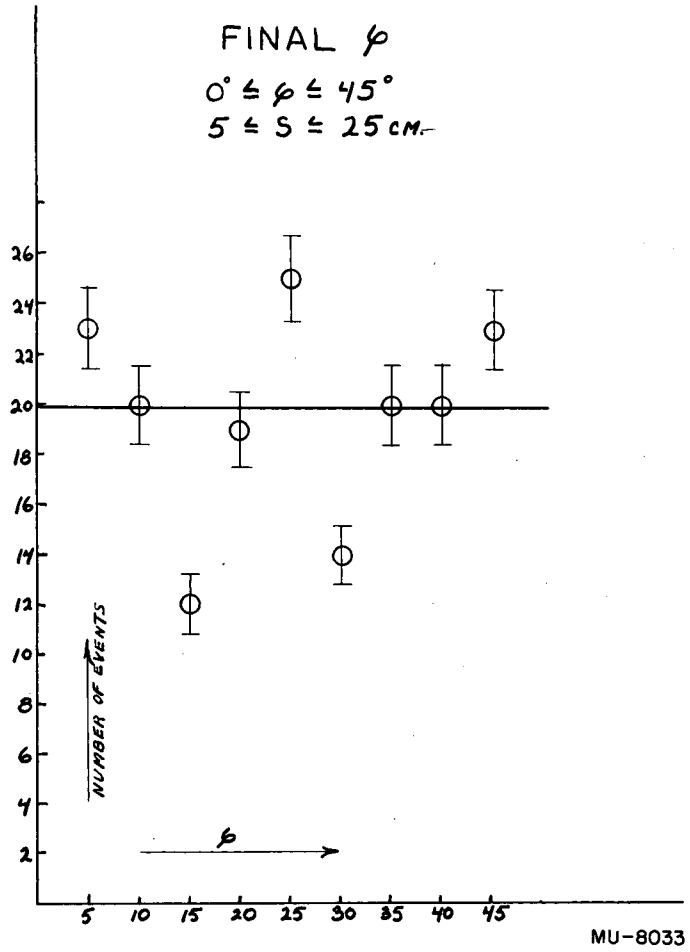

Fig. 14 Differential Azimuthal Plot Showing Number of Protons from Proton-Helium Elastic Scatters in 5^{o} Intervals of Azimuth.

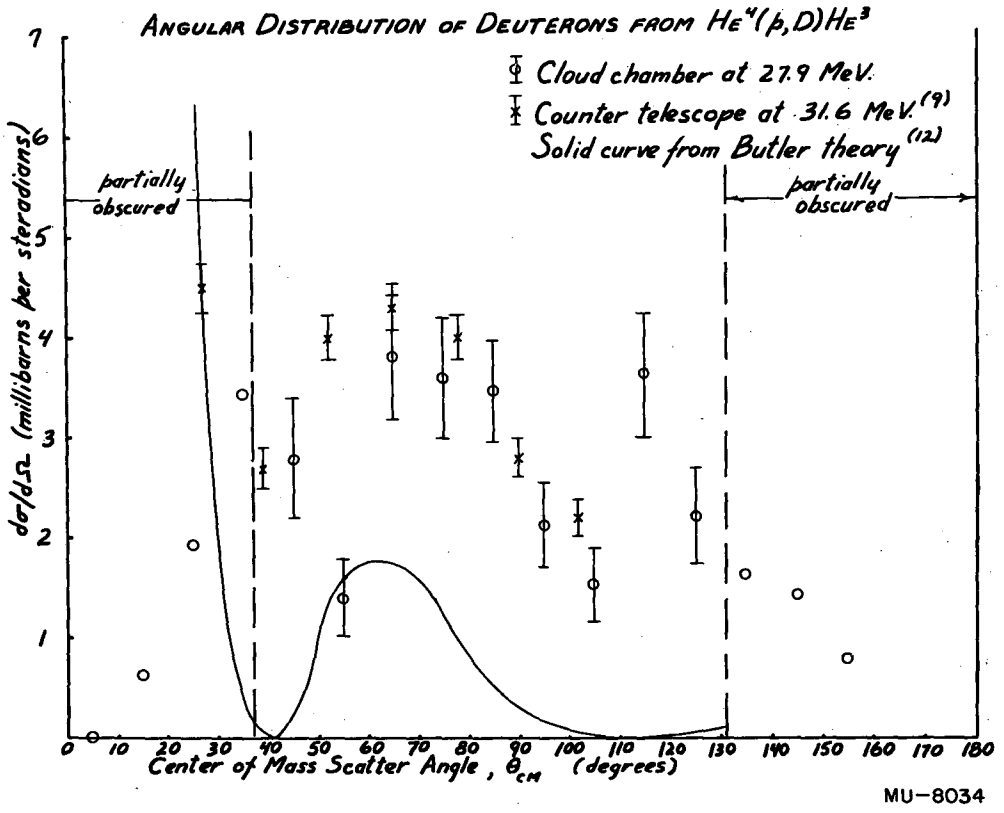

Fig. 15 Angular Distribution of Deuterons from He^4 (p, D)He^3, Cloud Chamber Data Taken in 10^o Intervals.

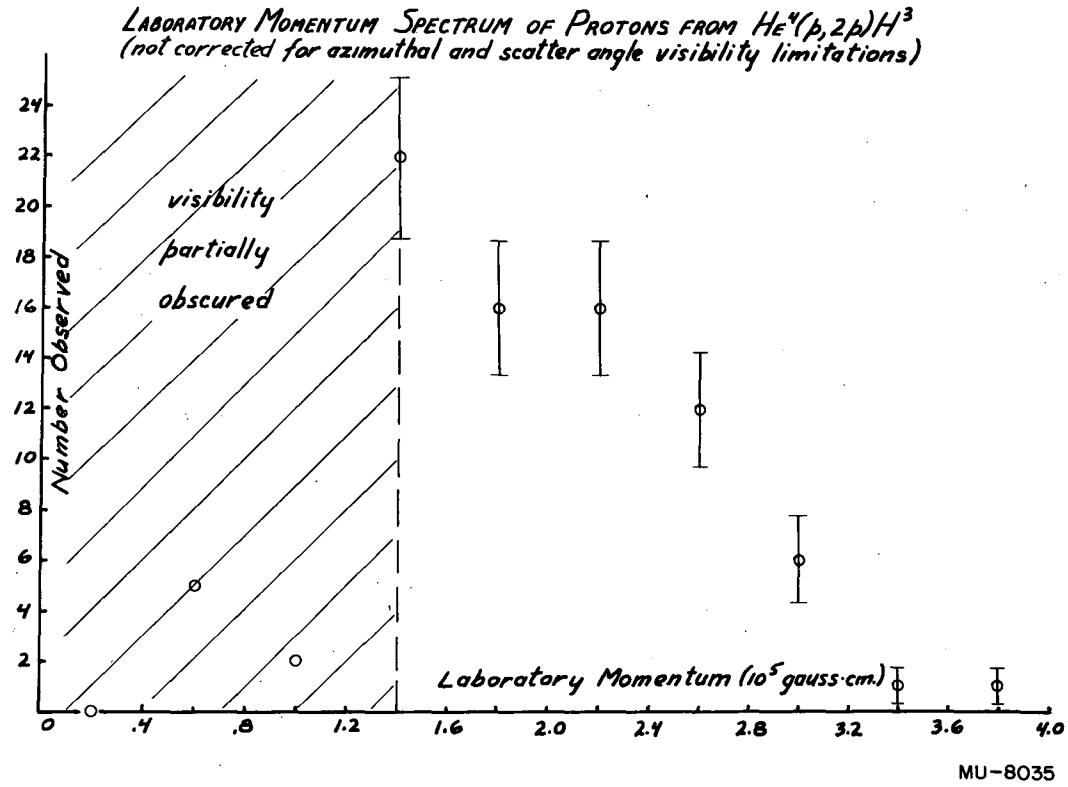

Fig. 16 Laboratory Momentum Spectrum of Protons from $He^4(p, 2p)H^3$ Reactions, Data Taken in 0.4×10^5 Gauss cm Intervals of Momentum.

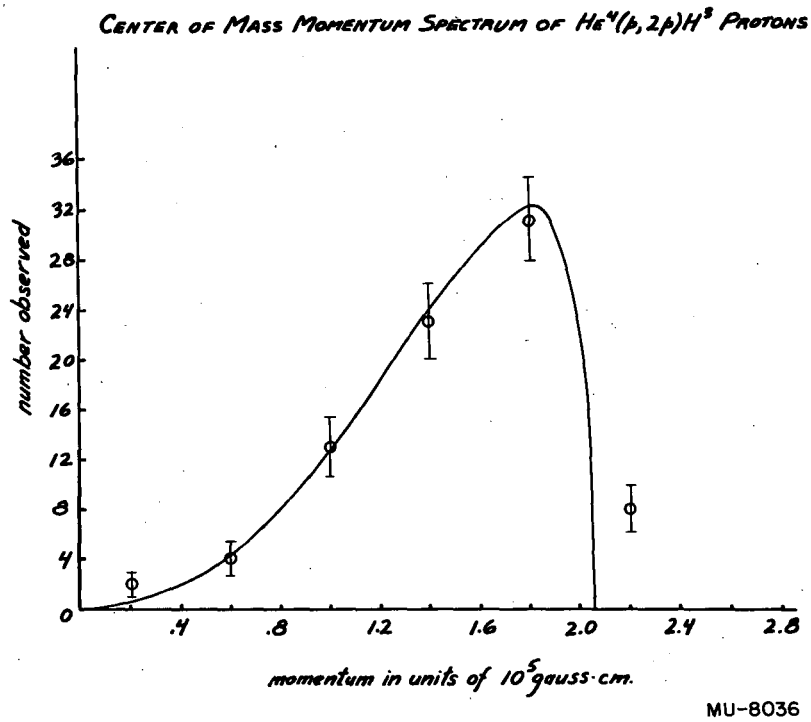

Fig. 17 Center of Mass Momentum Distribution of Protons from $He^4(p, 2p)H^3$, Data Taken in Intervals of 0.4×10^5 Gauss cm.

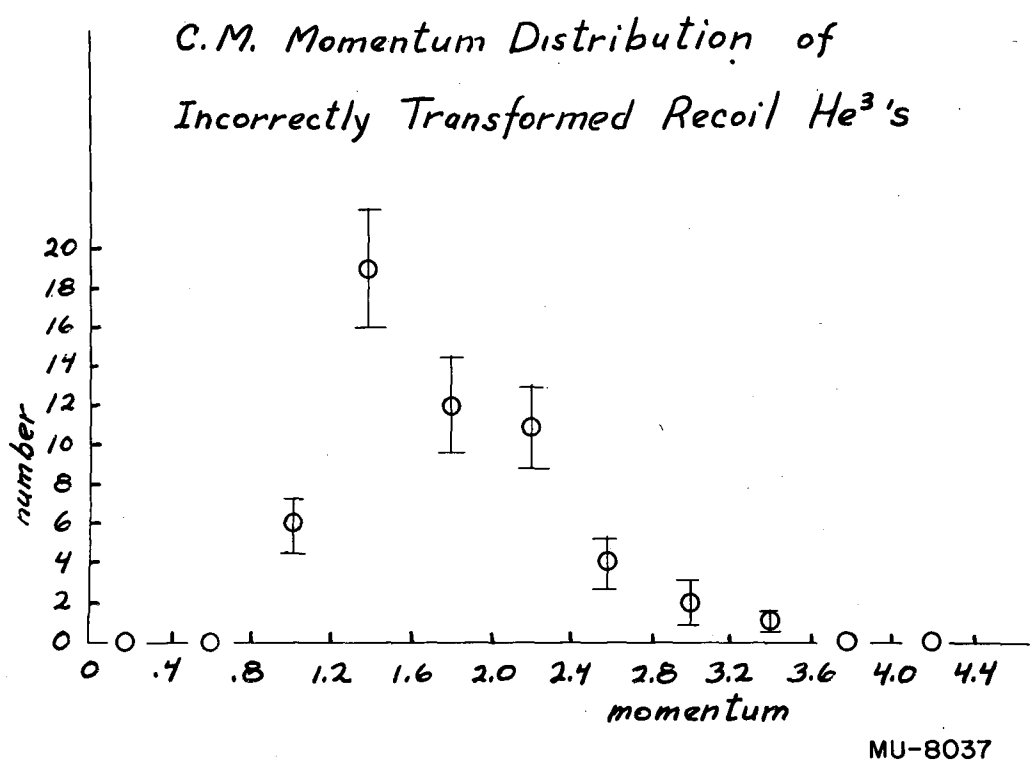

Fig. 18 C.M. Momentum Distribution of Incorrectly Transformed Recoil He^3's.

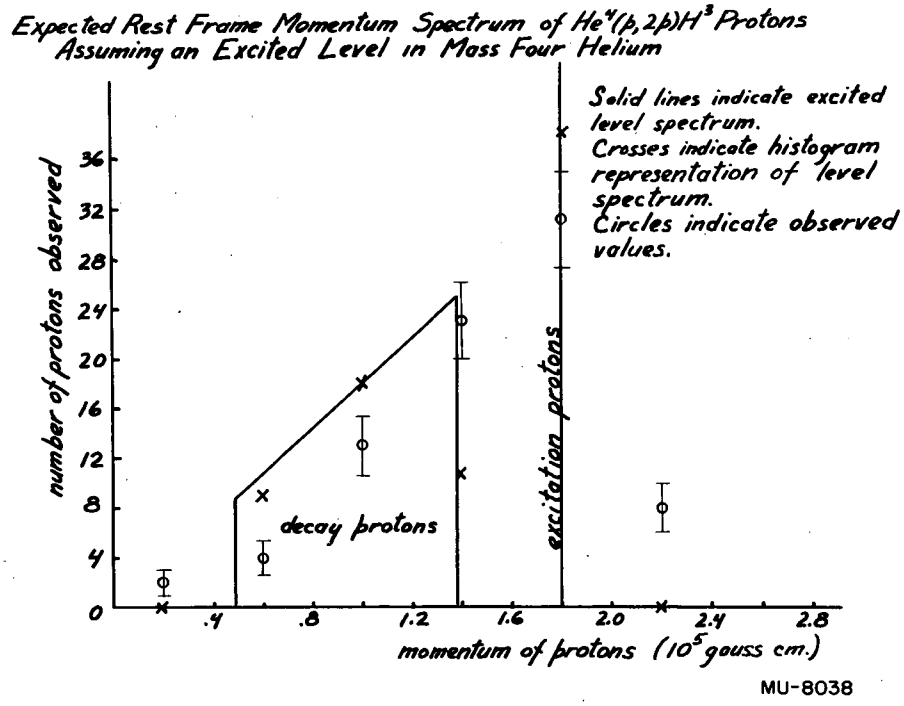

Fig. 19 Expected Center of Mass Momentum Spectrum of $He^4(p, 2p)H^3$ Protons Assuming an Excited Level in He^4.

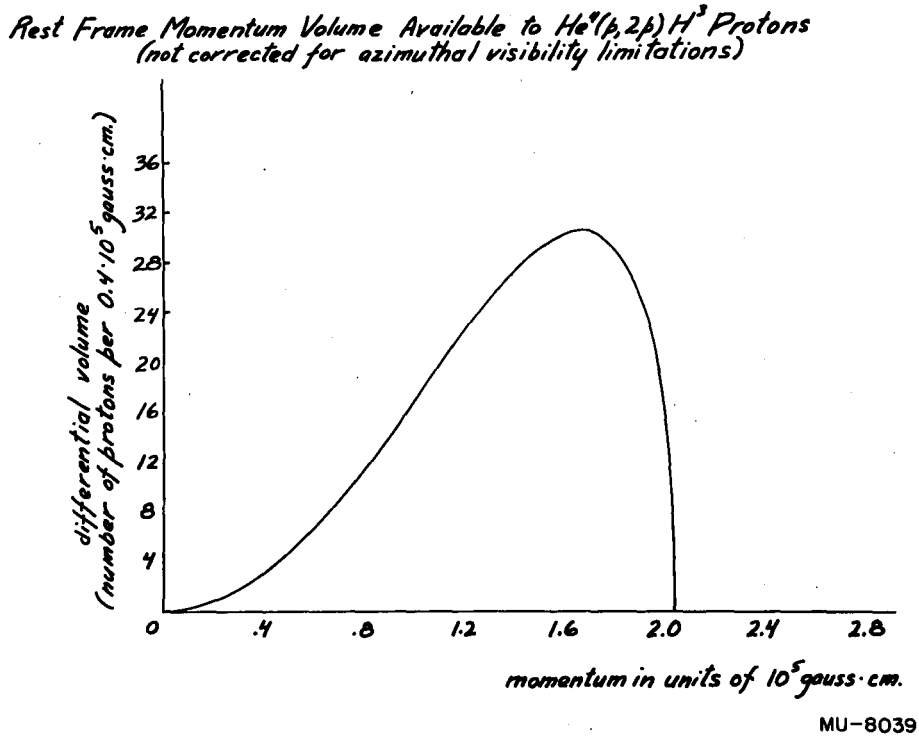

Fig. 20 Rest Frame Momentum Volume Available to $He^4(p, 2p)H^3$

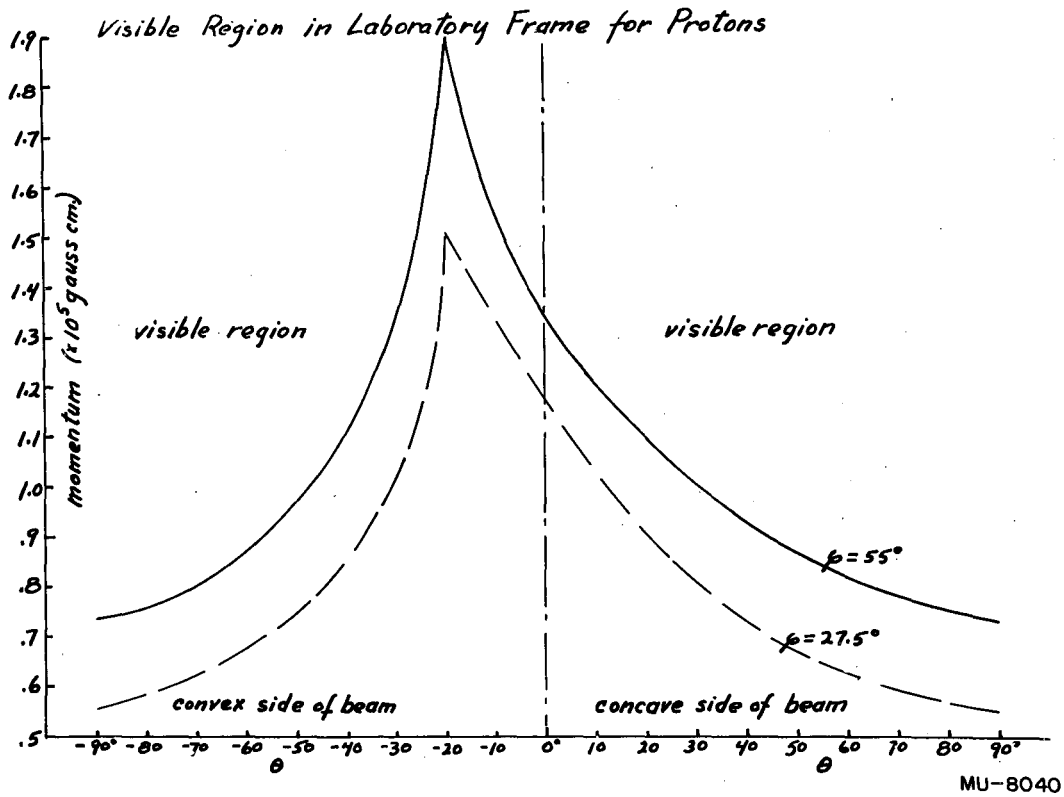

Fig. 21 Visible Region in Laboratory Frame for Protons.

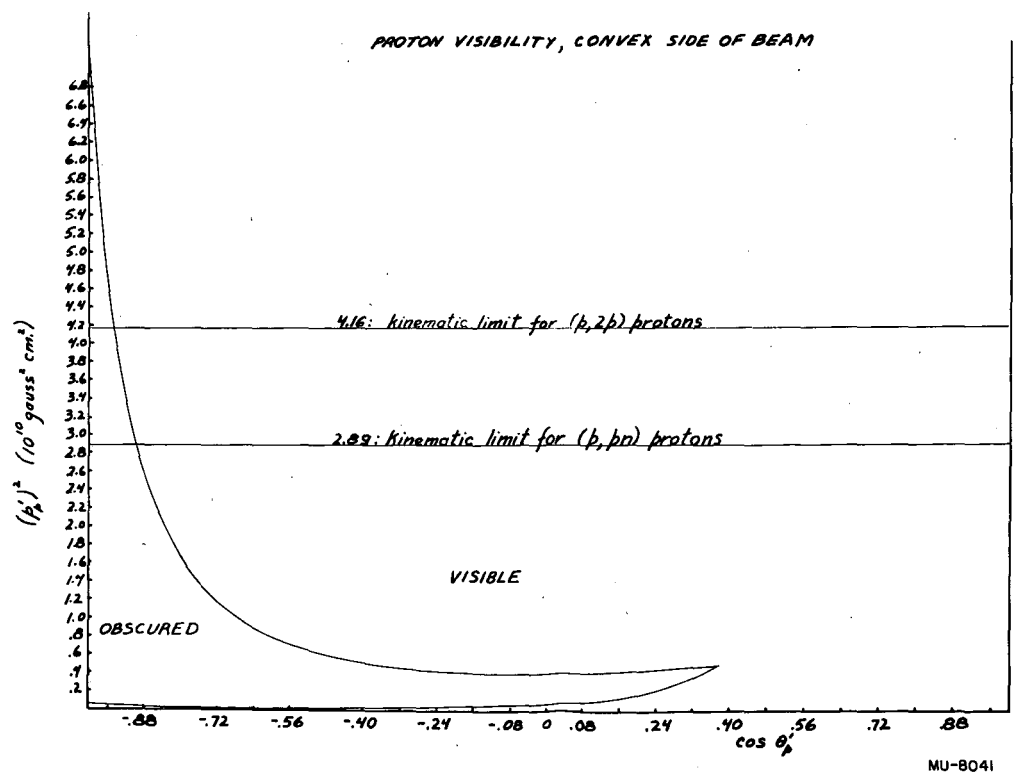

Fig. 22a **Mo**mentum Space Available to Protons.

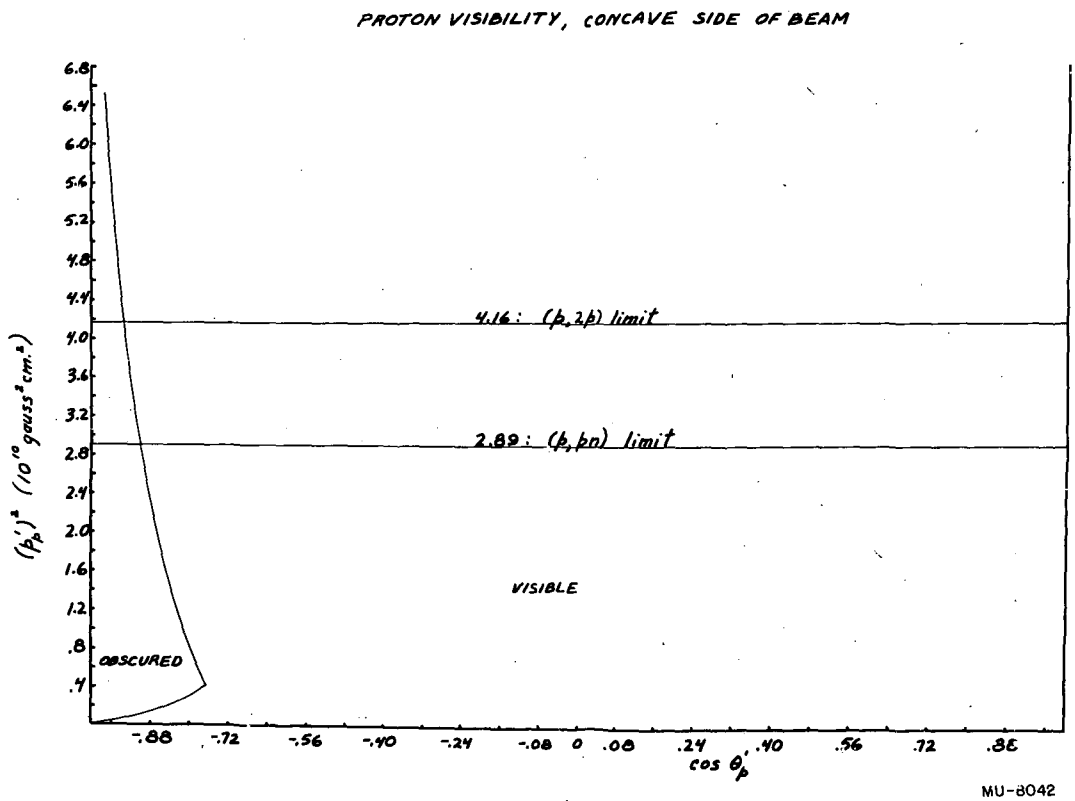
PROTON VISIBILITY, CONCAVE SIDE OF BEAM
6.8
6.4
6.0
5.6
5.2
4.8
4.4
4.0
3.6
3.2
2.8
2.4
2.0
1.6
1.2
.8
.4
$(p_p')^2$ (10^{10} gauss^2 cm.^{2})
4.16 : (p, 2p) limit
2.89 : (p, pn) limit
VISIBLE
OBSCURED
-.88
-.72
-.56
-.40
-.24
-.08
0
.08
.24
.40
.56
.72
.88
cos θ_p'
MU-8042

Fig. 22b

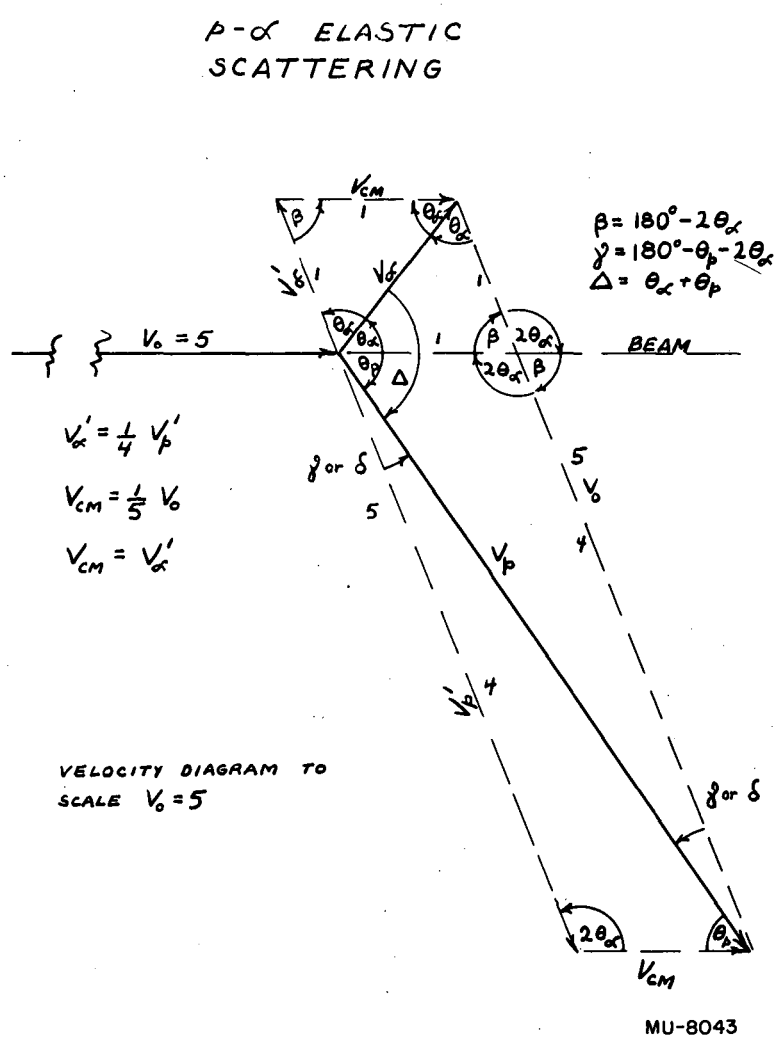

Fig. 23 Geometrical Diagram of p-α Elastic Scattering.

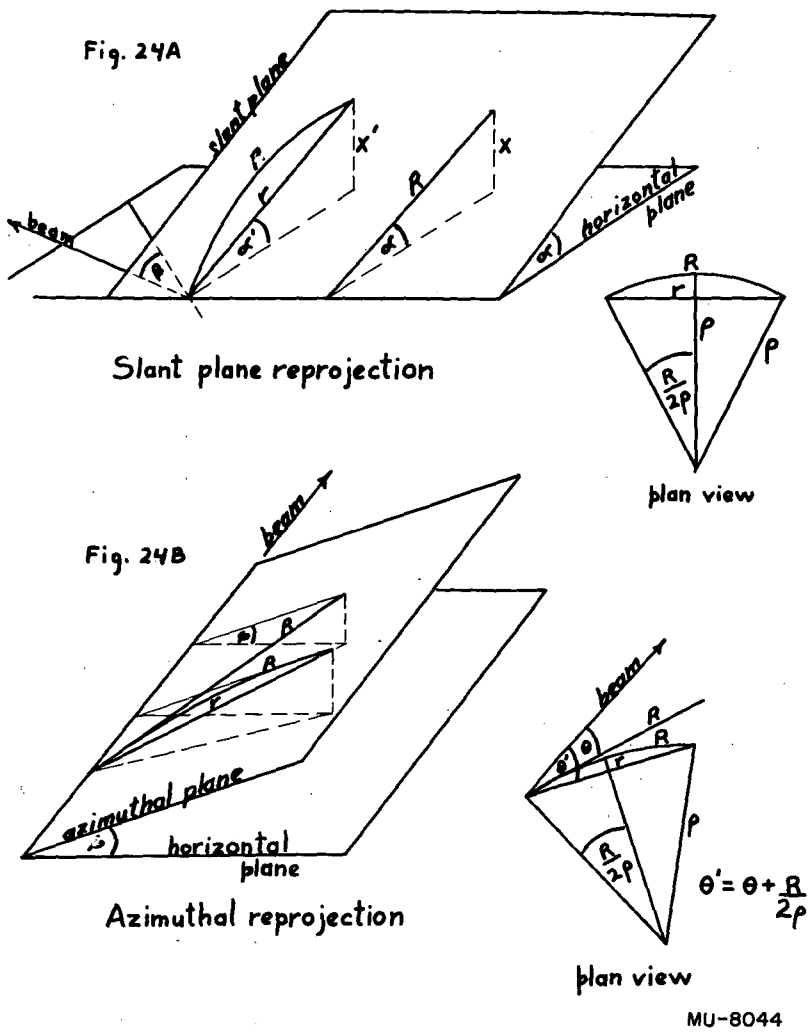

Fig. 24 Slant Plane and Azimuthal Reprojection.